Chapter 5

Scintillator detector fabrication

5.1 Overview

This Chapter describes the MINOS scintillator system. The first Section gives an overview of the baseline design. Section 5.2 sets the performance criteria for the scintillator system and Section 5.3 describes the interfaces of the scintillator system with other MINOS systems. Together, these first three Sections provide a complete overview of the scintillator system. Section 5.4 discusses in detail the elements of the scintillator WBS[1], including components, capital equipment costs, assembly procedures and calibration procedures. Finally, Section 5.5 discusses future engineering and optimization of the design.

5.1.1 Description of the scintillator system

The MINOS detector uses extruded plastic scintillator which is read out by wavelength-shifting (WLS) fibers coupled to multi-pixel photodetectors. This technique provides excellent energy and spatial resolutions. The baseline design relies only on existing technology for which performance measurements have been made. The major components of the scintillator system are:

- **Scintillator strips:** The active detector planes are composed of extruded polystyrene scintillator strips, 1 cm thick and 4.1 cm wide. Each detector plane is an octagonal array of 192 parallel strips. Each scintillator strip is co-extruded with a TiO_2 outer layer for reflectivity and a groove for a wavelength-shifting fiber. Several existing scintillator formulations and producers can meet MINOS specifications.

- **Fibers:** Wavelength-shifting (WLS) fibers are glued into a groove in each scintillator strip. In the far detector the fibers are read out from both ends, while the shorter near detector fibers are read out from only one end. Fibers with acceptable light output and attenuation are produced by Bicron and Kuraray. Figure 5.1 shows a sketch of a single scintillator strip with the fiber readout.

- **Scintillator modules:** The scintillator strips are assembled into either 20-wide or 28-wide (82 cm or 115 cm wide) modules for shipment to the near and far detector sites at Fermilab and Soudan. The shapes of the modules are designed to cover the

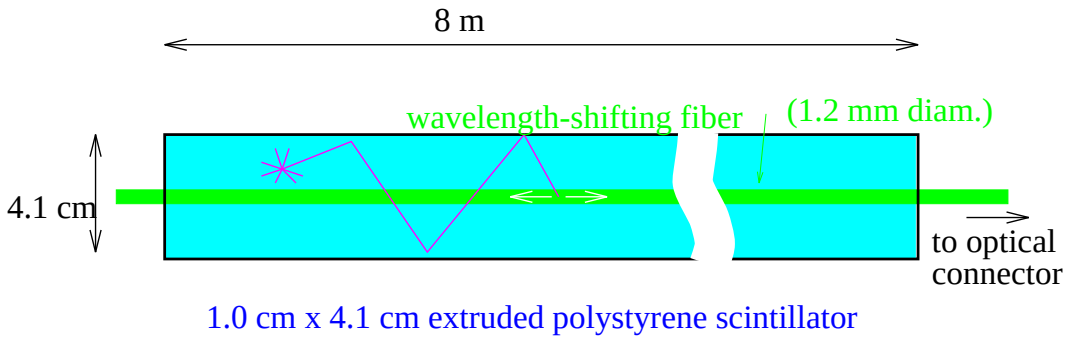

Figure 5.1: Sketch of a single scintillator strip. Light produced by the passage of particles is multiply reflected inside the strip by an outer reflective coating, and eventually may be absorbed inside the WLS fiber. The fiber re-emits light isotropically and some of this light is captured within the fiber and transmitted to the photodetectors.

octagonal steel planes. The strips within a module are glued to a light-tight outer aluminum skin, forming a rigid structure for easy handling and mounting. The ends of the modules have light-tight plastic manifolds which route the WLS fibers to bulk optical connectors.

- **Light guides to photodetectors:** Clear fiber ribbon cables carry light from the detector modules to multiplexing boxes where the photodetectors are mounted. Optical connectors are used for all fiber optics connections. The ribbon cables plug into the front faces of the multiplexing boxes.

- **Multiplexing boxes:** Each detector plane is divided into eight "logical modules." Each logical module consists of 24 adjacent strips (about 100 cm in width). Eight fibers, one from each of eight logical modules, are multiplexed onto a single photodetector pixel and its associated electronics channel. Demultiplexing is straightforward because the local order of fibers on one side of the detector is permuted with respect to the other side, giving unique patterns of light on the two sides. Each box serves two detector planes for one side, i.e., a total of three PMTs resides in a box. The 8-fold multiplexing is practical because of the limited spatial extent of neutrino events within a single detector plane. Figure 5.2 shows a schematic of the readout chain for the scintillator strips. Figure 5.3 shows a schematic of the multiplexing scheme.

- **Photodetectors:** The photodetector is the 16-channel Hamamatsu R5900U-00-M16 photomultiplier. These PMTs are housed in the multiplexer boxes and will couple directly to the front-end electronics. Each pixel of the PMT reads 8 signal fibers from different logical modules. A total of 24 pixels (1.5 photomultipliers) are required to read out each side of a detector plane. Figure 5.4 shows a schematic of how photodetectors are placed in the MUX boxes and interface to the electronics boxes. The assembly is modular and acts as a Faraday cage for the PMTs and electronics.

- **Calibration:** Calibration of the scintillator system is performed regularly using a combination of light injection to give the response curve of the photodetectors, and cosmic ray muons to normalize the response curve to energy. This necessitates an extrapolation over two orders of magnitude in light/energy. A calibration module, which can be placed in a test beam of hadrons and electrons, is used to determine the hadronic energy scale and the EM energy response and resolution. Radioactive sources permit quick checks on scintillator response.

Table 5.1 gives a summary of the scintillator system components.

Item	Each far plane	Each far supermodule	Full far detector	Near detector	Total
Number of scintillator planes	1	242	484	160	644
Area of scintillator [m^2]	53	12,800	25,600	2,400	28,000
Mass of scintillator [kg]	540	130,680	261,360	25,000	286,360
Number of scintillator strips	192	46,464	92,928	12,288	105,216
Length of scintillator strips [m]	1,293	314,200	628,400	60,000	688,400
Length of WLS fiber [m]	1,485	360,900	721,800	65,000	786,800
Number of 28-wide modules	4	968	1,936	224	2160
Number of 20-wide modules	4	968	1,936	320	2256
Number of M16 PMTs	3	726	1,452	588	2,040
Number of M16 PMT pixels	48	11,616	23,232	9,408	32,640
Number of readout channels	48	11,616	23,232	9,408	32,640
Number of MUX boxes	1	242	484	212	696
Number of 8-fold multiplexed pixels	48	11,616	23,232	-	23,232
Number of not-multiplexed pixels	-	-	-	9,216	9,216
Number of 4-fold multiplexed pixels	-	-	-	960	960
Length of (single) clear fiber [m]	1640	397,000	794,000	51,000	845,000

Table 5.1: Summary of basic quantities of the MINOS detector components. The values shown are approximations of exact engineering calculations.

Our choice of two-ended readout of the scintillator strips offers the following advantages:

- Better uniformity in light response from two ends, which may reduce systematic differences between the near and far detectors.
- Higher observed light level than with one-ended readout for the same scintillator light output.
- Redundant trigger capabilities, permitting detailed studies of trigger efficiency across the detector.

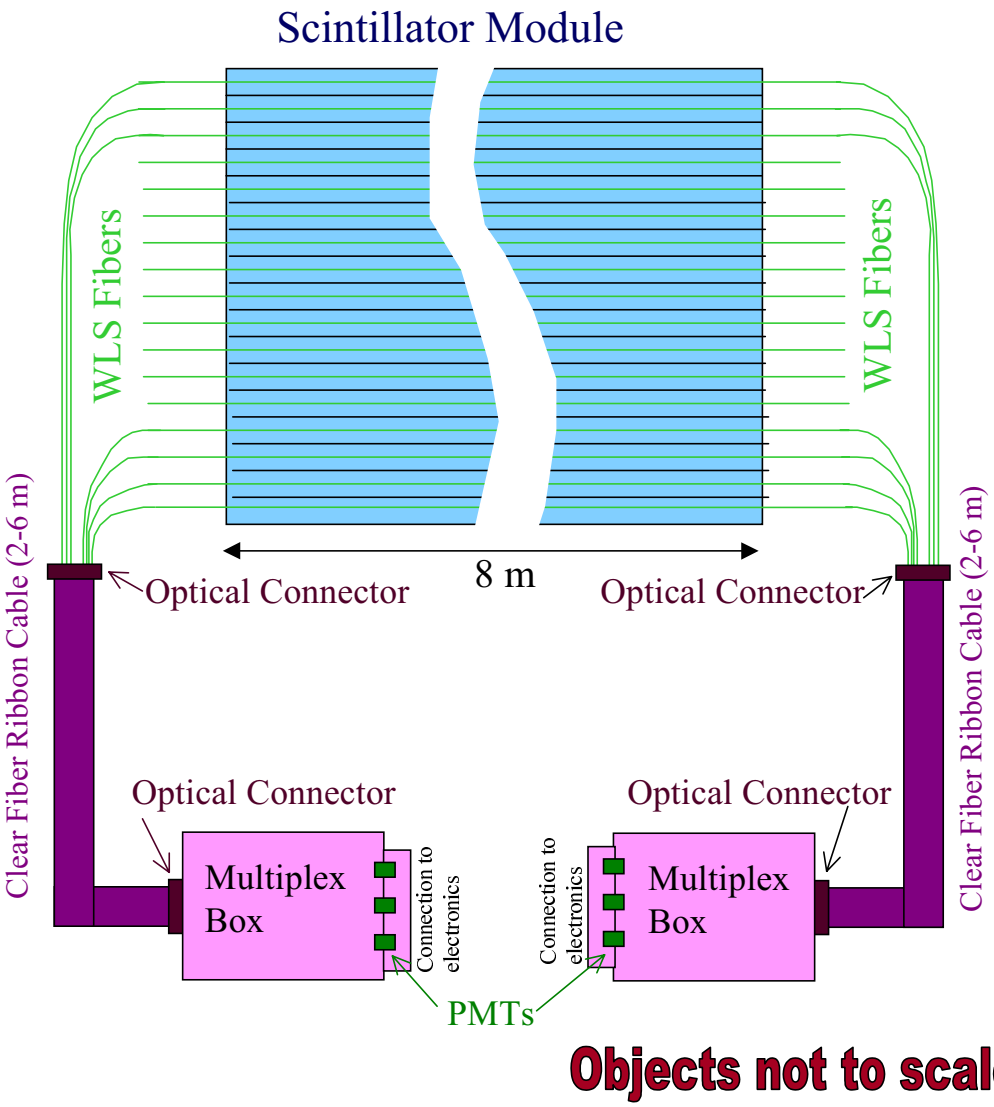

Figure 5.2: Schematic of the scintillator readout system. Modules (of two different widths) have WLS fibers routed to connectors at both ends. From there, light is routed through clear optical-fiber ribbon cables to a central location on each plane where the photodetectors are located. A fiber-routing "Multiplex" box then distributes the light from each scintillator strip to the appropriate photodetector pixel. There are eight modules in each plane of scintillator.

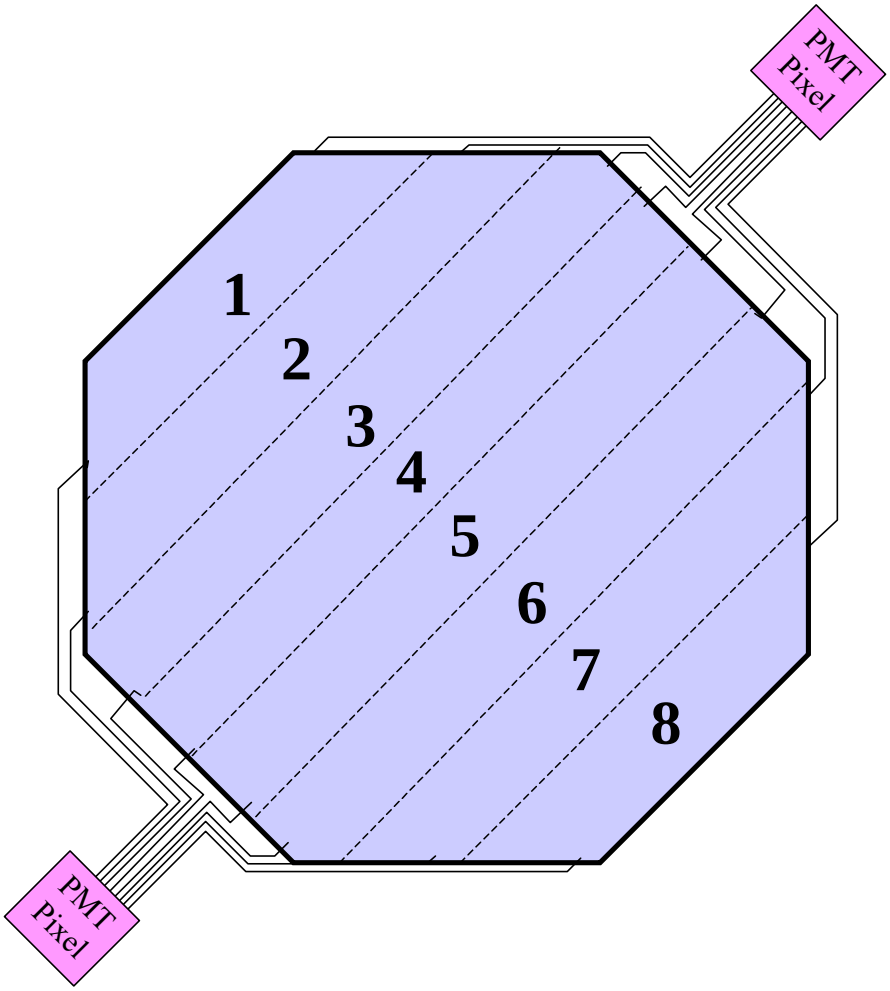

Figure 5.3: The MINOS scintillator system multiplexes eight fibers onto each PMT pixel. The multiplexing scheme combines one fiber from each of eight "logical modules" within a single scintillator plane. The fibers on a single pixel are separated by approximately one meter on the face of the detector. The pixel assignments of fibers on opposite sides of the plane are permuted with respect to the other side to permit demultiplexing in software. Because neutrino events are narrower than the 1 m multiplexing pitch, this approach saves money in PMTs and electronics without degrading sensitivity to neutrino physics.

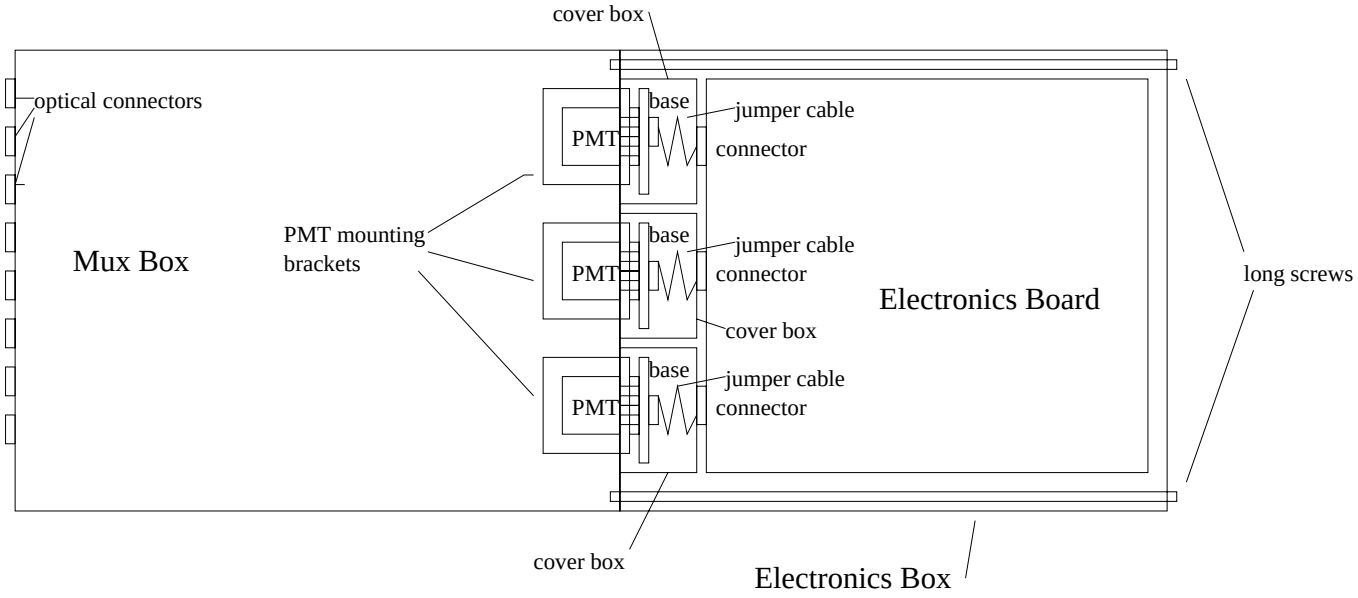

Figure 5.4: Sketch of the layout of a multiplexer box with phototubes and interface to the electronics. Both the multiplexer box and electronics are modular and the phototubes can be removed from the assembly in-situ by removing the electronics board.

5.1.2 Reasons for selection of solid scintillator

Solid scintillator has been used extensively in many particle physics detectors and in particular has frequently been the active detector of choice for sampling calorimeters. Extruded scintillator has already been employed in the D0 upgrade[2, 3]. Some of the features which make solid scintillator attractive are:

- **Good energy resolution:** We expect the energy resolution for 2.54 cm steel plates to be about $23\%/\sqrt{E}$ for EM showers and $53\%/\sqrt{E}$ for hadronic showers (E in GeV).
- **Excellent hermeticity:** There are very small gaps between strips.
- **Good transverse segmentation:** Analyses of simulated events show little improvement in physics measurement capabilities as strip widths are reduced below 4 cm. The baseline design uses 4.1 cm wide strips.
- **Flexibility in readout:** With solid scintillator, it is particularly easy to implement two-ended readout which offers several advantages as described above.
- **Fast timing:** Scintillation detectors have the intrinsic property of permitting nanosecond timing. This has advantages for the study of atmospheric neutrinos and permits a sensitive search for delayed signals in the neutrino beam.

- **Simple and robust construction:** Assembly of solid scintillator strips into detector modules requires little hardware and experience. Techniques for fiber connections have been completely worked out and implemented in major systems for both the D0 and CDF upgrades.
- **Potential for distributed production:** Because of the simplicity, the assembly and testing of complete modules could easily be distributed to multiple sites.
- **Long-term stability:** Our tests of extruded plastic scintillator show no serious aging or crazing problems. Since the stresses on the plastic are small in our design, crazing is not expected to be a problem in any case.
- **Ease of calibration:** A complete scheme for performing calibrations using a test-beam module, muons, laser pulses, radioactive sources and charge injection, has been designed and is described in this document.
- **Low maintenance:** We expect the system to be quite robust and to require little maintenance.
- **Reliability:** There are no catastrophic failure modes for solid scintillator which cannot be externally repaired. A possible long-term decrease in light output can be corrected using calibration data. Because there is little to go wrong, the detector is likely to achieve its intrinsic measurement capabilities.

5.1.3 Scintillator light output, transmission and detection test

In order to demonstrate the feasibility of the scintillator system we have constructed prototypes and measured their light output and uniformity using cosmic rays. All of the components related to the production, transmission and detection of light, which are described in this Chapter, were tested in the following prototype assembly. The setup consisted of two prototype scintillator modules, each with 16 strips. Other features included:

- 8 m long scintillator strips (1 cm $\times$ 4.1 cm wide, co-extruded with a reflective coating and with a WLS fiber groove). See Section 5.4.1 for a more detailed description.
- 1.2 mm diameter Kuraray wavelength-shifting fibers[4] were glued in the grooves using an the baseline optical epoxy (Epon resin and TETA hardener).
- End manifolds which route the appropriate lengths of WLS fibers from the strips to bulk optical fiber connectors.
- To simulate a real detector situation the wavelength shifting fibers were extended by 2 m by adding a 1.2 mm diameter clear-fiber ribbon cable running to a box housing the photodetectors. A connector was used on each end of the clear fiber cable.
- The light was routed to the photodetectors through an additional 40 cm of clear fiber inside the photodetector box.
- The photodetectors were 16-pixel Hamamatsu R5900U-00-M16 PMTs.

- The prototype module readout was triggered on cosmic rays by a system of external scintillation counters placed in several locations along the strips.

Figure 5.5 shows the mean effective light yield at each end and for the sum of the signals from both ends, expressed in terms of the number of photoelectrons registered by the Hamamatsu photomultipliers. The events for which the photoelectron yield is plotted were selected to be isolated minimum ionizing cosmic rays. The difference in the light levels on the two sides is due to different WLS fiber lengths extending beyond the ends of the scintillator strips on the two ends of the module. (The end with the longer WLS extensions gives lower light.) We observe that:

- The sum from both ends gives an average of more than 5.5 photoelectrons at all points along the scintillator strip.

- The light yield of the sum has a weak dependence on the distance from the end of the strip (i.e., the distance to a photodetector).

As described in Section 5.2, the observed light yield is adequate for MINOS. Specifically, the light yield is more than twice the minimum amount necessary for physics measurements, as determined by Monte Carlo simulations. This provides contingency for possible variation in, or degradation of, light output which might occur in the construction and operation of the experiment during its lifetime.

5.1.4 Calibration systems

Calibration of the hadronic energy response is of great importance in MINOS. In order to ensure a well-understood calibration at the required level of precision and accuracy, we will employ a combination of several calibration techniques:

- A test-beam calorimeter module for setting the overall energy scale and resolution.

- A combination of a light injection system and cosmic-ray muons for calibration of short-term and long-term variations.

- Radioactive sources for troubleshooting and to cross check other calibration methods.

Measurement of the total hadronic energy of events in MINOS is crucial to a complete set of neutrino oscillation measurements. The ability to measure Δm^2 precisely depends on the absolute calibration of the hadronic energy measurement. In order to reduce systematic limitations, we plan to calibrate the near and far detector hadronic energy responses to about 2% relative and 5% absolute uncertainty. Since it is impossible to illuminate the near and far detectors in-situ with high-energy hadron test beams, we must make careful use of several calibration tools to achieve this goal.

The fundamental calibration of the hadronic energy scale is achieved using a special calibration module for a series of test-beam and other calibration runs. Data are acquired in a test beam for muons, electrons and hadrons. Data from cosmic-ray muons, a radioactive source and light-injection are also collected during the test-beam running to help translate the calibration to the near and far detectors.

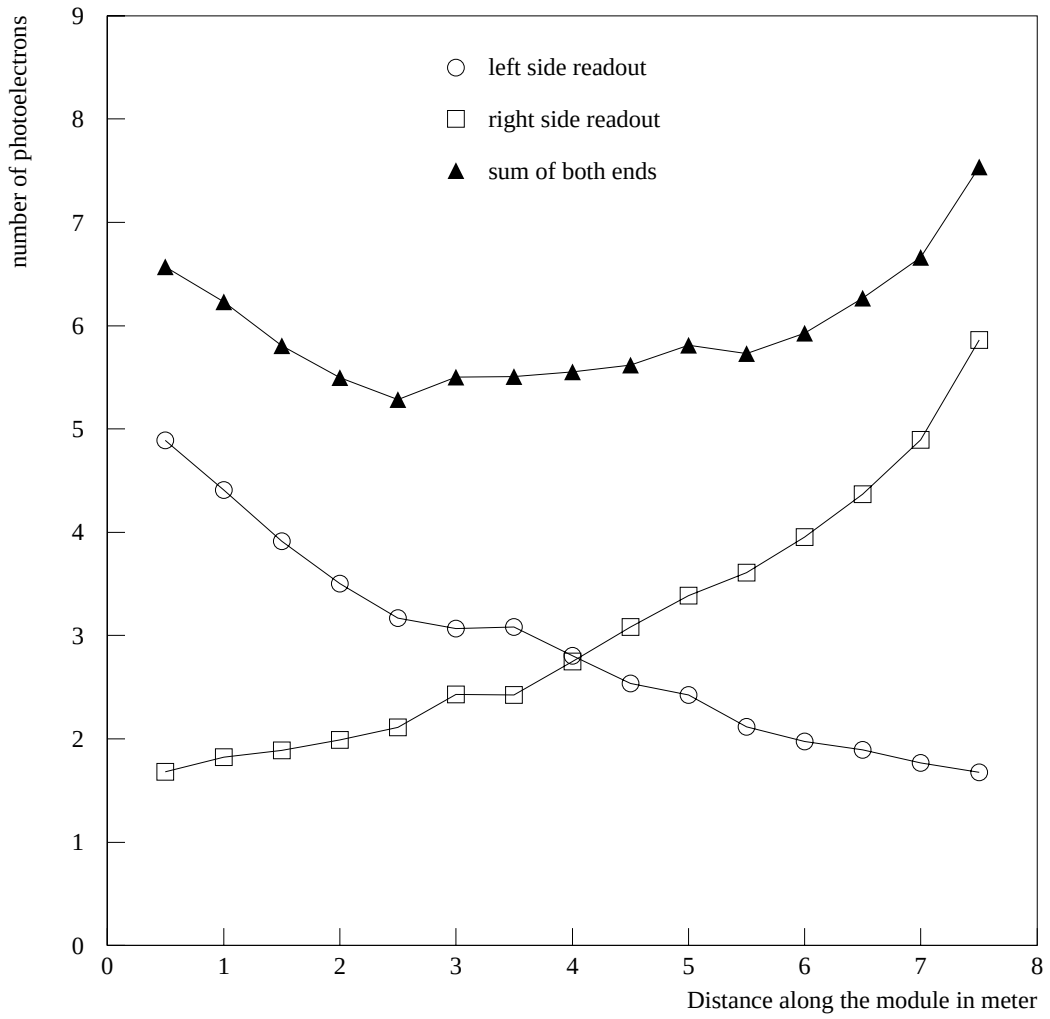

Figure 5.5: Results of photon yield measurements for single cosmic ray muons from a full scale prototype using 1.2 mm diameter fibers. The light measured at each end and the sum of the two ends is shown as a function of position along the strips. The difference in the light from the two ends is due to different lengths of WLS fiber extending beyond the ends of the scintillator strips.

Cosmic-ray muons provide the best means of calibration of the far detector and perhaps the best means of calibration for the near detector as well (although muons from upstream neutrino interactions may play as important a role there). The calibration is obtained by comparing muon energy deposition at different points in the detector with muon energy deposition in the test-beam module and hence with the hadronic energy data from the test beam. Due to differences in muon energies at the different depths of the detector sites, the calibration module could eventually be deployed at each detector site for a direct comparison of cosmic-ray muon data. This would ensure that there is no systematic error in translation of the test-beam calibration. The need to check for systematics of this type will depend on the outcome of neutrino oscillation measurements.

It is important to be able to track short-term variations in the response of the system. Light is injected into the WLS fibers to measure the response of the photodetectors and electronics through the full dynamic range of the system. This is one of the two main functions of the light injection system. The second function is to identify any connector or fiber problems. In addition to the light injection system, the electronics is calibrated by direct charge injection (see Chapter 6).

Muons provide the energy normalization for the light injection system. Because it requires about a month of muon data per strip at the far site (much less time is needed at the near site) to provide an absolute calibration, the light injection system is used to keep the photodetector gains approximately constant during the time over which the muons are recorded.

The responses of all scintillator modules are mapped in detail using a radioactive source during module construction. In addition, a tube which can hold a radioactive source is installed at each end of every scintillator module to permit insertion of a wire source, after the detector plane has been installed, for short-term cross checks on other calibrations and debugging at installation time.

5.1.5 Description of the scintillator factories

Construction of the components for the scintillator system requires a few different types of "factory" operations. Most of these operations are quite compatible with resources and skills available in collaborating laboratories and universities while some require industrial production. Many of the basic components of the system are already available as "catalog" items. Examples include the photodetectors, WLS fiber and clear optical fiber.

Some of the other components require specialized industrial production based on specific requirements for MINOS. Examples of these items include the scintillator strips, the end-manifold and coil bypass components of the scintillator modules, and bulk optical connectors. We have carried out an extensive development program for extruded scintillator over the last year in order to develop an industrial product which meets our light output demands for an acceptable cost. At present, we have a production technique which involves a cooperative effort between MINOS and an industrial extrusion house, Quick Plastics[5]. Since this industry is not experienced in the production of scintillator and the subtleties of measurement of light output, we envision a continued cooperative effort for production of scintillator for MINOS. In addition, two commercial producers of plastic scintillator (Kuraray[4] and Polycast[6]) have been actively pursuing production of extruded scintillator. Kuraray has delivered scintillator of good quality and continues their development program. We are in

close contact with both of these companies to ensure that their products will meet the specifications of the scintillator for MINOS. Because these products are not yet finalized, we assume here that the production will be via a direct cooperative effort of our own technical staff with industrial plastic extruders. However, we expect that Kuraray and Polycast will be able to provide comparable products and we will evaluate bids for production when we are ready to place orders.

The three main systems which must be fabricated "in house" by MINOS are the scintillator modules, assembled clear-fiber ribbon cables (with connectors attached and polished) and multiplexing boxes which house the photodetectors and route light from signal fibers to the appropriate pixels on the photodetectors. The assembly of the scintillator modules requires the most manpower and equipment.

The scintillator modules could be produced at a single production site running two shifts per day. However, we expect that the optimal production scenario will include two factory locations for module production. This permits faster production (or contingency in the schedule) and more efficient use of collaboration resources while keeping costs low. Attractive features of the assembly of plastic scintillator modules are that the cost of specialized assembly equipment is relatively low, the space required for assembly is not particularly large and the level of skill required in the assembly is relatively low. The necessary space, skills and oversight capabilities exist at several collaborating laboratories and universities.

The production of scintillator modules involves the following major steps:

1. Gluing WLS fibers into scintillator grooves.
2. Assembly of strips into 20-wide and 28-wide modules.
3. Routing of fibers through the end manifolds and into the bulk optical connectors.
4. Potting and polishing of optical connectors.
5. Closing the completed assemblies and checking for light leaks.
6. Mapping of modules using radioactive sources.

Specialized machinery and fixtures have been designed to facilitate this work.

The production of optical fiber ribbon cables and boxes to house photodetectors require relatively simple equipment, readily available in most laboratory and university shops. The only specialized equipment needed are assembly jigs and fly cutters for polishing of optical connector faces.

We plan to begin routine production of scintillator components for MINOS detectors in October 2000. The first commercial orders for various components would precede this by several months.

5.2 Requirements and performance criteria

The technical requirements on the scintillator system have been set from a combination of physics studies, general considerations about detector response and practical considerations. They are:

1. **Light output:** The light output must be sufficient so that the hadronic energy resolution is better than $60\%/\sqrt{E}$ and that the efficiency for observation of a muon crossing a strip is greater than 90%. This is expected to be the case as long as the total number of observed photoelectrons per minimum-ionizing particle crossing a scintillator layer is greater than 2.5 with discrimination at the single photoelectron level. A factor of about 2 times more light than this (5.0) is desirable to account for assembly variation and aging of components. The current baseline design meets this requirement. To the extent that higher light output will help with other technical considerations (e.g., noise levels), higher light output will be pursued as long as the overall cost of the detector is not significantly impacted.

2. **Uniformity:** In order to ensure that it is possible to correct for position dependence of showering events, the light output of the scintillator strips should vary by no more than 30% with respect to a nominal response at that location (after correcting for attenuation in the WLS fiber).

3. **Attenuation:** The light observed from the near and far side of a strip (by the detector at the near end) should differ by no more than a factor of 5.

4. **Timing:** The time resolution from the sum of strips within a scintillator plane should be less than 2 ns for 10 pe's and 5 ns for 2 pe's.

5. **Stability:** The light output of the scintillator system should have long-term stability with an expected decay-time of at least 10 years. Short-term variations must be measurable so as to permit relative energy calibration for hadronic showers between the near and far detectors at the level of 2%.

6. **Calibration:** The hadronic energy response should be able to be calibrated to a relative error between the near and far detector of no more than 2% up to at least 30 GeV. An absolute calibration of 5% will be made using a test beam measurement.

7. **Linearity:** The detector response to hadronic showers should be linear to within 5% between 1 GeV and 30 GeV.

8. **Crosstalk:** The crosstalk between scintillator channels should be less than 4%.

9. **Transverse pitch:** The scintillator strips should be 4 cm in width for pattern recognition on EM showers.

10. **Modular construction:** The scintillator strips must be assembled into modules which are easy to handle, relatively rugged and provide light-tight seals.

11. **Cost:** The cost should be as low as possible given the above considerations. The overall cost of the scintillator system should be reviewed with respect to other detector costs prior to final production in order to produce a best overall optimization of physics capability.

5.3 Interfaces to other MINOS systems

Interfaces between the scintillator system and the other MINOS systems have been defined as follows:

- The scintillator fabrication task provides the scintillator modules, clear optical cables, multiplexer boxes, phototubes, HV bases and the various calibration hardware.
- Scintillator modules mount to the steel using mounting bars at the ends and straps attached to plates welded to the steel at intermediate points. The scintillator modules are designed to be mounted on the steel prior to lifting the steel plane into place.
- The interfaces between the scintillator system and electronics system are the mechanical and electrical connectors between the multiplex boxes and the electronics modules. High voltage for the phototubes is provided from these modules by the electronics task.
- Packing and shipping of scintillator modules is part of the scintillator system production responsibility. Handling of the modules at the near and far detector sites is the responsibility of the installation tasks.
- All test and calibration equipment for the scintillator system (including their use during installation) is the responsibility of the scintillator task.
- The cavern outfitting task provides the rack platforms, located along the 45° faces of the octagons, for mounting the scintillator multiplexing (MUX) boxes and electronics racks and modules. The scintillator task is responsible for production and testing of the MUX boxes and the clear fiber cables between the modules and MUX boxes. Installation and in-situ testing of the MUX boxes and cables is the responsibility of the installation tasks.
- The general experiment database system provided by the electronics task is used to manage various construction and calibration information. Data from assembly and testing of scintillator modules are stored in this database for use during installation and analysis. Scintillator modules are marked with bar codes for reading at installation time. The bar-code reader and associated software are supplied by the scintillator task.

5.4 Description of WBS elements

5.4.1 Scintillator strips (WBS 2.2.1)

The recent development of extruded scintillator which can be inexpensively mass produced in very long strips is one of the reasons that solid scintillator can be used in MINOS. The production of extruded scintillator for MINOS has built upon work done by Fermilab in conjunction with the D0 upgrade[2, 3].

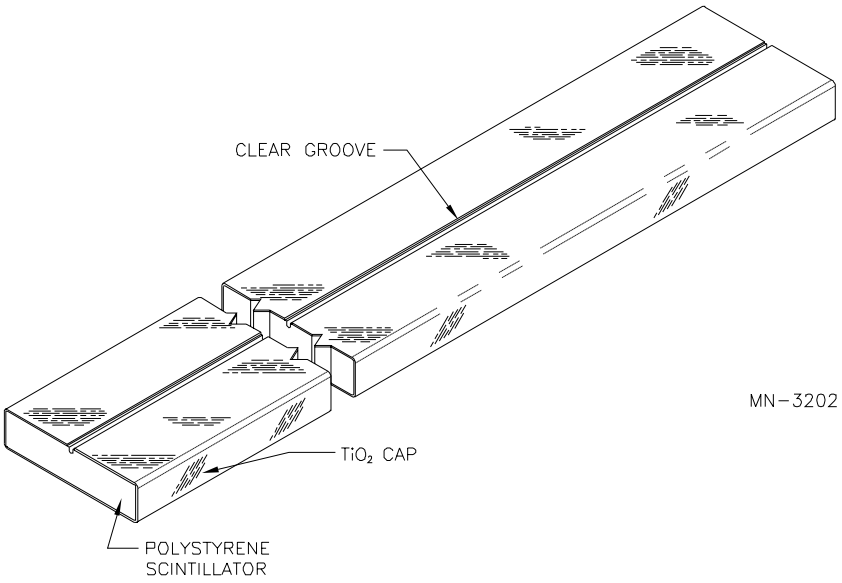

Figure 5.6: Sketch of a scintillator strip with groove and reflective coating.

5.4.1.1 Description of scintillator strips

The scintillator strips are made of polystyrene, infused with the fluors PPO (1%) and POPOP (0.030%). This compound is melted and extruded in the shape of a rectangular bar with a narrow groove along the center of one of the wide sides, as shown in Figure 5.6. The groove is 1.3 mm deep, sufficient to contain a 1.2 mm diameter wavelength-shifting fiber. A thin (0.25 mm thick) reflective jacket, composed of TiO_2 infused in polystyrene, surrounds the entire scintillator bar except for a small region near the groove. Each scintillator strip is 4.1 cm wide, 1.0 cm thick, and up to 8 m long, as shown in Figure 5.7.

Traditionally, the manufacturing of scintillator strips has been accomplished in two steps; first mixing fluors into polystyrene, extruding that mixture and letting it cool and then in a later step re-melting the scintillator mixture to extrude strips of a specified shape. In the last year, we have developed a one-step process where the fluors are infused with raw polystyrene pellets in the same machine which is used to extrude final scintillator strips. In test production, this technique has proven to be reliable and cost effective and we have now specified it as the baseline. We consider the two-step process to be a contingency option in case scaling up the one-step process proves too difficult.

In the one-step or "in-line" production process, fluors are first tumbled with dry polystyrene pellets which have been held under an argon atmosphere for several days prior to extrusion. The PPO and POPOP are pre-measured into convenient packages for addition to a set amount of polystyrene pellets during the mixing process. The mixture of pellets and fluors are fed into an extrusion machine which melts the polystyrene, allowing the fluors to

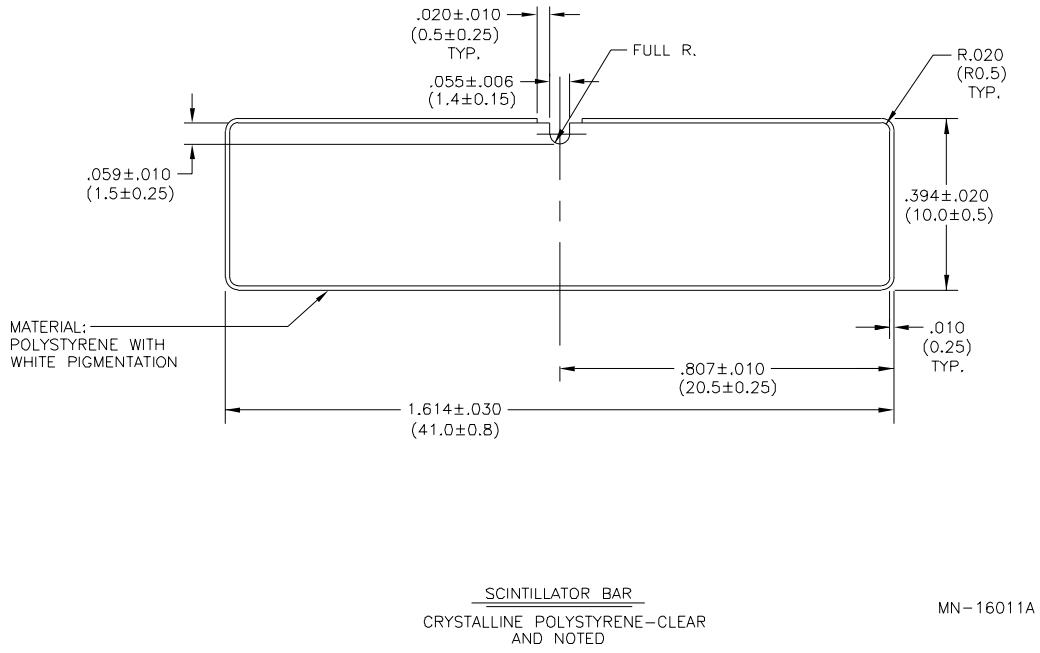

Figure 5.7: Detailed cross-section of a scintillator strip.

diffuse uniformly. The scintillator mixture is extruded through a die to produce the desired strip cross section. As the scintillator is extruded through the die, the outer reflective coating of polystyrene mixed with TiO_2 (10% by weight) is added through material injected from a second, "satellite" extrusion machine which mixes the polystyrene and TiO_2. As the plastic emerges from the die, it is further formed using vacuum sizing and cooled with air and water. The scintillator is extruded continuously and strips are rough cut to lengths of 8.0 and 11.3 m.

The total weight of plastic scintillator to be installed in the near and far detectors is approximately 630,000 pounds. We estimate that it will require 720,000 pounds of raw polystyrene to produce all of the scintillator strips because of inefficiencies in the extruding and cutting processes. About 42% of the scintillator strips on the far detector are 8 m long. The remainder are between 8 m and 3.3 m long, as the octagonal shape of the detector dictates. By cutting a single 11.3 m long strip into two sections, it is possible to keep the amount of waste material small and still have each strip of exactly the right length for its octagon location. The length of near detector strips ranges from 1.5 m to 4.0 m. Scintillator strips are rough cut at the extruding facility and are cut to the exact lengths required at the module assembly factories.

The commercial production of this quantity of scintillator strips is within the capacity of typical commercial extruders over a 2 year time span. Faster production could be accomplished by having additional extrusion machines operating in parallel. However for our expected needs a single machine is sufficient. We currently have contracts with two extruding

companies, Quick Plastics[5] and Royalite Thermoplastics[6], to produce prototype scintillator strips for MINOS. Kuraray has also expressed interest in the scintillator production for MINOS as has Vladimir Technoplast in Russia.

5.4.1.2 Performance measurements

It is important to understand the light production, collection and uniformity properties of extruded plastic scintillator. These properties will vary with factors such as the shape of the strip, reflective coating and clarity of the material. We must also determine the uniformity which can be achieved during actual mass production of extruded strips.

The TiO_2-loaded co-extruded layer on the strips requires less manpower than wrapping strips with a reflective material such as Tyvek. We have extruded the strips both with and without the TiO_2 coating to measure the reflection efficiency of the coating compared to Tyvek. We found no observable difference in the amount of light collected with the TiO_2 compared to Tyvek, making the co-extrusion an attractive and cost-effective reflector.

We have compared the collection of light from a WLS fiber laid in an extruded groove on the broad side of a scintillator strip with that from a fiber placed in an extruded hole in the center of a scintillator strip. A dry (unglued) fiber in the groove yields about 10% less light than a dry fiber in the hole. However, for our geometry and scintillator material, we find that a fiber glued in the groove yields 1.8 times more light than a dry fiber. Since gluing is much easier in a groove than a hole, we have chosen to glue fibers in grooves for our baseline design.

Our studies of the aspect ratio of scintillator strips (width and thickness) have shown that, for 1-cm thick extrusions, a 2-cm wide strip gives about 1.3 times more light than a 4-cm wide strip. Simulations of neutrino events show that changing from 2-cm to 4-cm strips has very little effect on physics capabilities. The lower light yield of 4-cm strips still meets MINOS requirements, and the cost is lower than for narrower strips. We have therefore chosen 4-cm wide strips for the baseline design. The optimal aspect ratio may be sensitive to the reflectivity of the outer surface and to the clarity of the polystyrene to scintillation light; we are continuing our studies of these effects.

For the baseline scintillator strips, we have measured a number of strips for uniformity in the light output, both along the strip lengths and transverse to their long axes.

1. Longitudinal uniformity

   We have studied the uniformity of the light output of several scintillator strips by measuring photomultiplier tube current while moving a beta source along the strips. The measured light output at each location has been corrected for the fiber attenuation. The results are shown in Figure 5.8 for strips which were intentionally taken from different times of an extrusion production run. The variation in the light collection efficiency of the WLS fiber at different locations is negligible. Hence, the 13% spread in the measurements is probably due to the nonuniformity of the scintillator strips and the variation in optical coupling between fibers and strips.

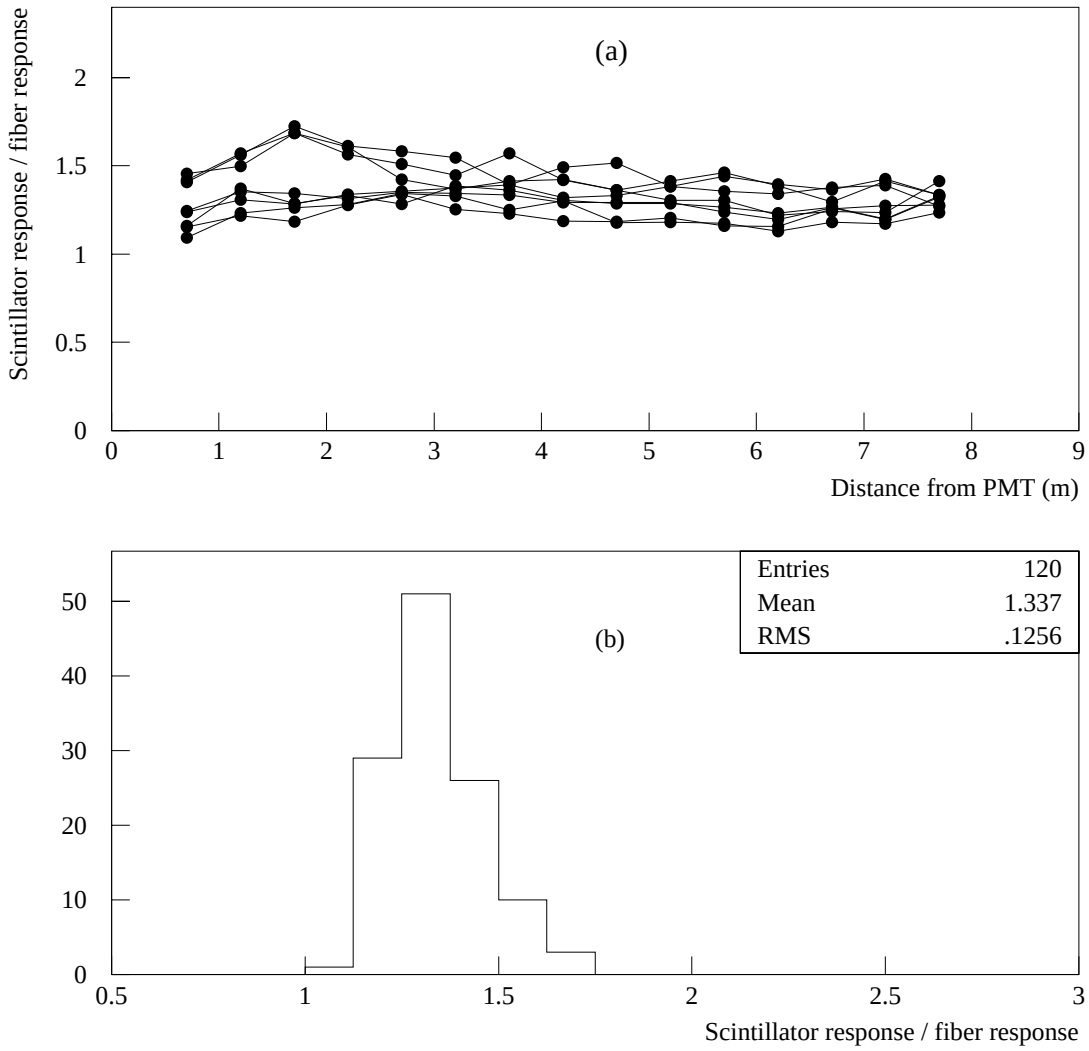

Figure 5.8: Scintillator longitudinal uniformity: Responses of the scintillator strips (arbitrary normalization), corrected for fiber attenuation, are plotted versus the position in (a), and the projection is histogrammed in (b).

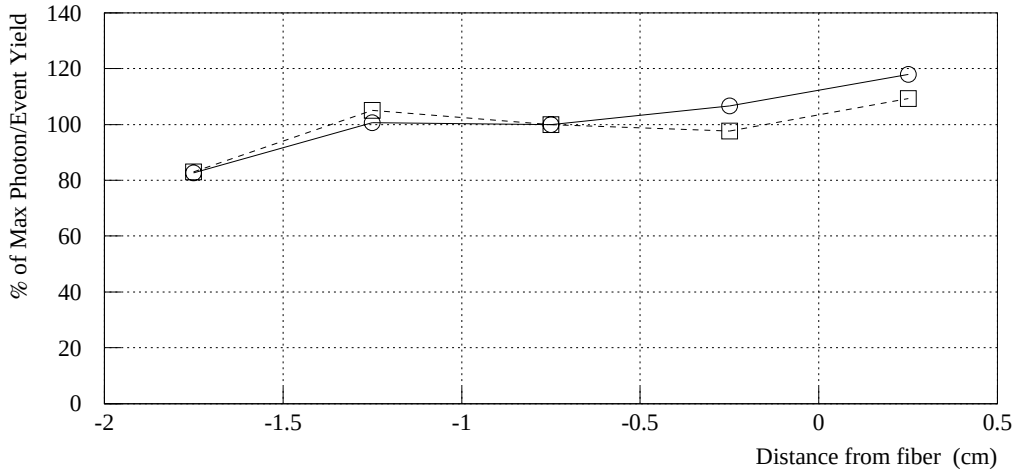

Figure 5.9: Scintillator transverse uniformity.

2. Transverse uniformity

   We have measured the uniformity of the light output of scintillator strips transverse to their lengths using cosmic-ray muons. The muon trigger consisted of two narrow scintillators above and below the scintillator strips. Measurements of two strips are shown in Fig. 5.9. The light output decreases by about 20% near the edge, mostly due to the fact that the thickness of the scintillator in these extrusions was slightly smaller near the edge. This was the result of an early production process; all of our commercial extruders have assured us that final scintillator strips will have no such variation. We expect our final strips to have thickness uniformity to better than about 5%.

5.4.2 Fibers (WBS 2.2.2)

5.4.2.1 WLS fibers

The wavelength-shifting (WLS) fibers which shift the blue scintillation light to green are a critical component in the overall light collection scheme. Blue photons produced in the scintillation process make many reflections from the highly reflective outer layer of the co-extrusion. The blue photons eventually hit a fiber where they are absorbed by the WLS Y-11 fluor and re-emitted as green photons. The absorption spectrum of the Y-11 fluor, centered at a wavelength of 420 nm (blue), has only a very slight overlap with the emission spectrum, centered in the green beyond 470 nm, so that self-absorption in the fiber is small. The fibers then act as light guides to channel the green light, through optical connectors and lengths of clear fibers, to the photodetectors. This provides a very efficient means of "focusing" the light into a small-area photodetector, whose cost is roughly proportional to photocathode

area. This is one of the main features which makes scintillator readout practical for MINOS.

Measurements and Monte Carlo calculations have been used to study the various factors affecting light collection: i.e., reflectivity of the outer co-extrusion, and scintillator/fiber sizes and geometry. We have chosen to use 1.2 mm diameter fibers which maximize the use of the available area of photocathode on the PMT and give the required light output with our extruded scintillator strips. The total length of WLS fiber required (including allowance for spares and waste) is about 850 km. The fibers are double-clad to give a maximum trapping fraction for the green light: the inner core containing the WLS fluors is polystyrene (refractive index $n_1 = 1.59$), a thin intermediate layer is acrylic ($n_2 = 1.50$) and the thin outer cladding is a polyfluor ($n_3 = 1.42$). For green light produced on the axis of a fiber, the fraction of light trapped and traveling in one direction is given by $(n_1 - n_3)/2n_1$. This factor is 5.5%. Both experiment and photon-bookkeeping have verified that this simple treatment is correct. (Light produced off-axis has a greater trapping fraction, but these rays are attenuated more rapidly.)

One of the most crucial properties of the WLS fiber for determining the light yield at the photodetector is its effective attenuation length when the source of green light is remote from the photodetector. MINOS requires a very large number of fibers with lengths in excess of 8 m, significantly longer than the requirements of any previous experiment. We have made measurements of many fibers from the two vendors, Bicron[9] in the U.S. and Kuraray[4] in Japan. Performances of some batches of WLS fibers are shown in Figure 5.10. All of the fibers measured from the batches represented here are acceptable for use in MINOS. The results shown here come from three different batches of fiber, two from Bicron and one from Kuraray. The Bicron fibers are all 1 mm diameter BCF91-A while the Kuraray fibers are all 1 mm diameter, double-clad, non-S-type fibers with 150 ppm Y-11 fluor. (Although not shown, we have measured that 1.2 mm diameter fibers have the same attenuation length as 1.0 mm diameter.) The batches of Bicron fibers represent production of about 2000 m of fiber while the Kuraray fiber was from a 100 m sample. Further orders have been placed to study possible variation in larger production batches. The better batch of Bicron fiber represents a newer production of that fiber. We conclude that either of these manufacturers can supply fiber of high quality for MINOS. The Kuraray fibers are somewhat stiffer than the Bicron fibers and require somewhat more space in the end-manifold design.

Aside from the differences in the absolute light output in different batches, all WLS fibers show similar characteristics. The attenuation is approximated quite well by a sum of two exponentials: one with a short attenuation length of less than 1 m and one with a much longer attenuation length of 5 to 6 m, the crucial component for MINOS. The short component is due to self-absorption of the green light in the WLS fiber and the short attenuation length agrees reasonably well with emission and absorption data provided by the manufacturers.

We have found that different batches made months apart can have significantly different values for the longer attenuation lengths. The best long attenuation length that we have measured is 10.5 ± 0.5 m, in fibers from Bicron. This appears to be the best ever produced by that company, and also appears to be the longest attenuation length reported in the literature. It seems likely that this is the best that can be achieved and may represent the limit set by the properties of the polystyrene core of the fibers. The attenuation length of MINOS WLS fibers must be at least 5.0 m.

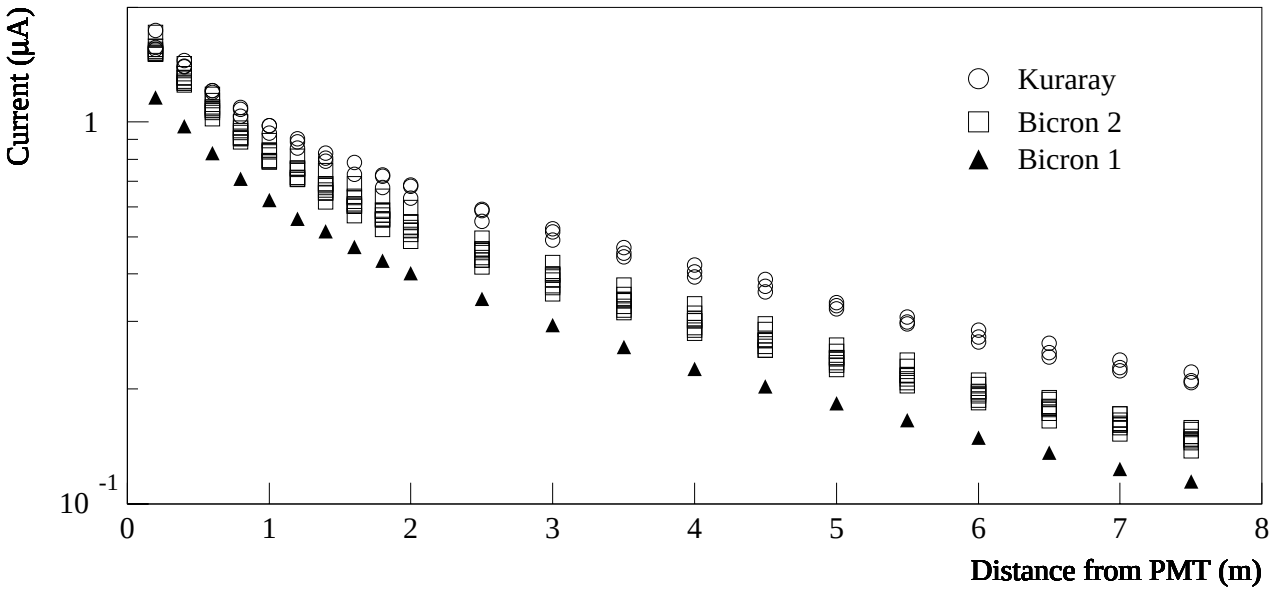

Figure 5.10: Light collection and attenuation in WLS fibers. The current from a phototube is measured as a scintillator is placed at various positions along the length of the fiber. Bicron 1 and Bicron 2 are two batches produced in the summer and fall of 1997 respectively. The Kuraray batch was produced in December of 1997. All results shown here are acceptable for MINOS. See text for additional details.

5.4.2.2 Clear fibers

Clear-fiber ribbon cables are used to transmit light from the WLS fibers to the multiplexing boxes. We plan a similar approach as used for construction of these ribbon cables for the CDF endplug upgrade[10]. MINOS ribbon cables consist of eight or ten clear fibers enclosed in an outer black plastic coating which provides protection and light tightness. Mitsubishi offers a cable of this type and has provided a quotation for production for MINOS purposes. The fibers are 1.2 mm diameter, double-clad polystyrene, manufactured by Kuraray, and are spaced 2.3 mm apart. When coupled to WLS fibers, the clear fiber cables act as extensions of the WLS fibers, but with better attenuation length. (Hence, more light is observed than if a similar length of WLS fiber were used.) The attenuation length of clear-fiber cables has been measured to be 12 m for light which is already collimated (as it is coming from a few meters along a WLS fiber)[11].

The clear fibers are routed along the edges of the steel detector planes, from the scintillator modules to the MUX boxes. The routing for the far detector is shown in Figure 5.11. This routing minimizes the length of clear fiber required while keeping readout isolated be-

tween scintillator planes. The total length of clear fiber required for construction of the ribbon cables for both the near and far detectors is about 1022 km, slightly more than the total length of WLS fiber.

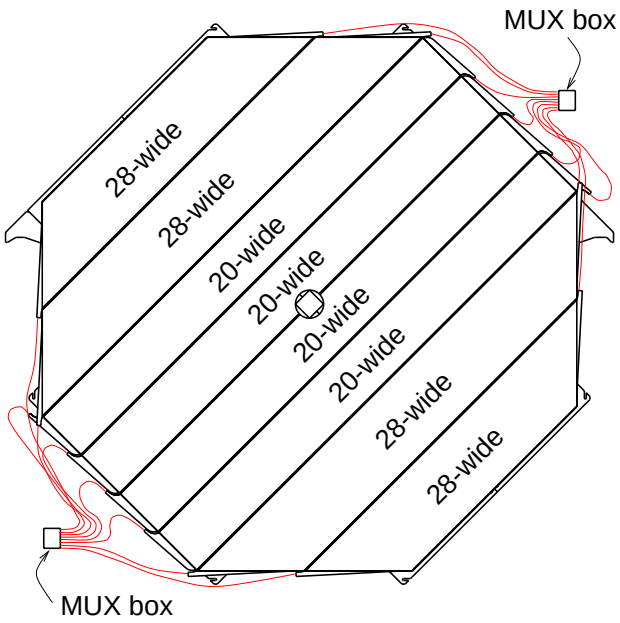

Figure 5.11: Clear fiber routing and scintillator module layout for readout of one view of scintillator modules for the far detector. Each octagon has eight modules with bulk optical connectors at each end.

5.4.3 Scintillator modules (WBS 2.2.3)

5.4.3.1 Design features and requirements

The baseline design simultaneously optimizes several different concerns:

- Gaps between individual strips are kept as small as practical.
- The scintillator fully covers the steel in order to keep the fiducial mass as large as possible.
- Scintillator modules are designed to be light-tight and permit rapid testing.
- Light-fiber connections to the scintillator modules use reliable bulk connectors.
- The mechanical design of the modules gives good light output and long-term stability.
- Assembly work at the near and far detector sites is kept to a minimum in order to permit rapid installation. A modular design of preassembled and pretested strips is ideal for this purpose.

- Total costs for production of scintillator modules are minimized by balancing capital equipment, component, manpower and shipping costs and use of existing resources.
- Assembly operations and equipment are simple, and permit production and testing of modules in both national laboratory and university facilities, staffed by local physicists, students and technicians.

All of these features have been achieved in the design described here. The modules are either 20 or 28 strips wide glued to a thin aluminum skin which provides mechanical strength, light-tightness and fire protection for the polystyrene scintillator. Wavelength-shifting fibers are routed to 28-wide bulk connectors at each end of the module through a simple manifold which curves the fibers through a natural bend radius, protects them from harm and provides a light-tight enclosure. The components have been designed to be rugged and permit easy assembly and handling of the modules. The thin aluminum skin permits mapping of the scintillator modules with radioactive sources to test for any problems in the assembly. Fibers are glued into the scintillator strips to maximize light output. The modules are mounted onto the steel plates using a simple steel-strap technique which permits very narrow gaps between neighboring modules and a minimal gap between steel plates.

5.4.3.2 Overview of module construction

This Section provides an overview of the hardware architecture of a plane of scintillator strips in the far detector. The packaging of scintillator strips into light sealed modules is described first. End manifolds, which route WLS fibers to optical connectors at the end of each module, are discussed next. Hardware used to attach the modules to the steel absorber planes is then described.

Each plane contains a total of 192 scintillator strips. All of these strips have an identical 4.1 cm by 1 cm nominal cross section, as described in Section 5.4.1. However, the lengths vary from 1.5 m to 8 m to match the octagonal shapes of the near and far detector absorber planes.

The scintillator strips are grouped into modules of 20 or 28 strips strips each, yielding a total of 8 modules per plane. The number of strips has been set to permit four 20-wide modules in the center of each octagon and two 28-wide modules on each outer side of the octagon. The layout of the modules on a plane is illustrated in Figure 5.11. The modules are enclosed in aluminum cases to provide a light-tight seal.

A total of four separate module geometries are required for one plane. Two styles of modules have ends angled at 45° to their length. The next module style has perpendicular ends; all strips in this style are 8 m in length. The last style also has perpendicular ends, but requires a bypass at its center to provide clearance for the magnet coil. The same parts are used for the different styles to minimize the number of unique parts required and to maximize assembly efficiency. For example, the two styles having 45° ends differ only in length; both lengths use the same end manifold components.

The parts comprising a module can be subdivided into three functional groups. The first is the scintillator strips themselves. By the time of assembly into a module, the WLS fibers and reflective extrusion groove cover have been glued to the strips, as described in Section 5.4.3.3. Second, a two-piece light seal and structural box is included about the entire

periphery of a module, as described in Section 5.4.3.4. Third, an end manifold assembly routes and protects the WLS fibers extending from the ends of the scintillator strips; the components in the manifolds are described in Section 5.4.3.5.

The innermost two modules have a fourth functional component: the bypass assembly to accommodate the magnet coil. The bypass is described in Section 5.4.3.8.

The scintillator modules are fastened and supported on the steel plane using several techniques, as described in detail in Section 7.4.3.2. Eight meter long modules are fastened to the absorber planes at the end manifolds and at four equally-spaced points along their length. (Some of the shorter modules do not require all four intermediate mounts.) Further support is provided by a shelf positioned at the bottom 45° edge of an absorber plane (shown as the bottom right 45° edge in Figure 5.11). The hardware used to tie the modules to the planes is described in Section 5.4.3.9.

5.4.3.3 Coupling of fibers to scintillator

In prototype tests with extruded scintillator strips, we have found that a significant improvement in light collection is achieved when fibers are glued into the scintillator strip rather than just being placed into a dry groove or hole. For the baseline strips and fibers, we find a consistent factor of 1.8 more light observed at the photodetector for fibers glued into the grooves compared to fibers placed into grooves dry. This is independent of the position along the strip/fiber assembly. Hence, we have decided that in MINOS, fibers will be glued into grooves. It should be noted that in some previous applications of WLS fiber readout of scintillators (tile calorimeters for instance) no significant difference has been observed in the light output when fibers were glued. This is the result of differences in materials and geometry between those detectors and the extruded strips for MINOS.

We have tested several glues which meet MINOS requirements. We have chosen a very cost effective glue which has properties very similar to those of Bicron 600 epoxy (which has been used extensively in other detectors) but at about 1/8 the cost. The baseline glue is Shell Epon 815C resin[12] with triethylenetetramine (TETA) hardener mixed at 100 parts to 13 parts by weight). We have performed assembly and aging tests using this glue and have confidence that it will meet our needs. One concern with use of glue is possible aging and yellowing. Previous aging measurements on BC-600 glue over a 5 year period have shown it to be quite resistant to yellowing, and it does not attack WLS or clear fibers[13]. We have performed our own accelerated aging tests using Bicron 600 and the baseline glue and found them to have very similar performance (with the baseline being slightly better).

1. Optical properties: The index of refraction of the Shell Epon glue is very close to that of polystyrene. This good match ensures minimal loss of light at the scintillator-glue interface, helping to give the factor of 1.8 in increased light collection. The light transmission in the wavelength region of interest is measured and is shown in Figure 5.12. Assuming very conservatively that the light from the scintillator traverses an effective thickness of 500 μm of the glue before reaching the fiber, 1% or less of the light will be absorbed by the glue.

2. Mechanical properties: We have glued several tens of fibers into scintillator strips and have observed no signs of the glue failing to create a good optical bond in normal

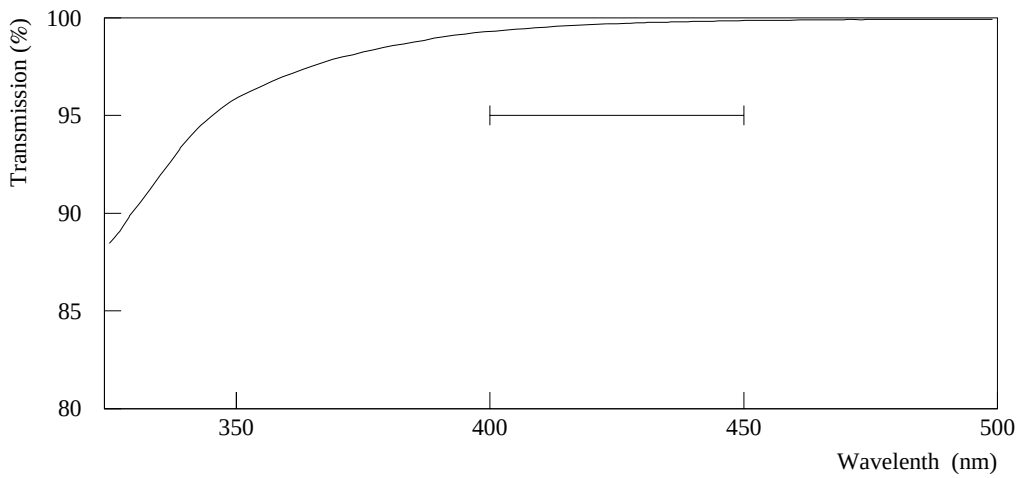

Figure 5.12: Transmission spectrum of 500 μm thick Shell Epon 815C optical cement (with TETA hardener). As a reference, the range of light spectrum emitted by the scintillator and absorbed by the WLS fiber is indicated.

handling. Furthermore, we have subjected some strips to severe mechanical handling and bending with no observed reduction in light collection. We have also subjected some glued strips to repeated severe temperature cycling with no suggestion of the glue releasing from the scintillator.

3. Reflective extrusion groove cover: We have found that aluminized Mylar works very well as a reflective cover above the groove. It can be applied as the fiber is glued in and improves the light collection by about a factor of 1.15 compared with no reflective cover.

5.4.3.4 Light case

Each module is enclosed in a sheet aluminum light case to shield the scintillator from external light and to protect the flammable polystyrene strips from ignition sources. The architecture of the light cases is described here; fabrication and assembly information is provided in Section 5.4.8.3.

The light case is fabricated from 0.5-mm thick 3003H14 aluminum sheet, provided by the manufacturer on a coil. The coil stock is flattened and rolled into shallow U-shaped channel sections (where the bottom of the U is the module width) at each module factory. Two U channels are used to fabricate one case, with the top being slightly narrower than the bottom. The bottom U channel is positioned on the module assembly table and filled with 20 or 28 scintillator strips. The top U channel is positioned over the scintillator strips and nested in the bottom U channel. Figure 5.13 shows a short section of the top and bottom

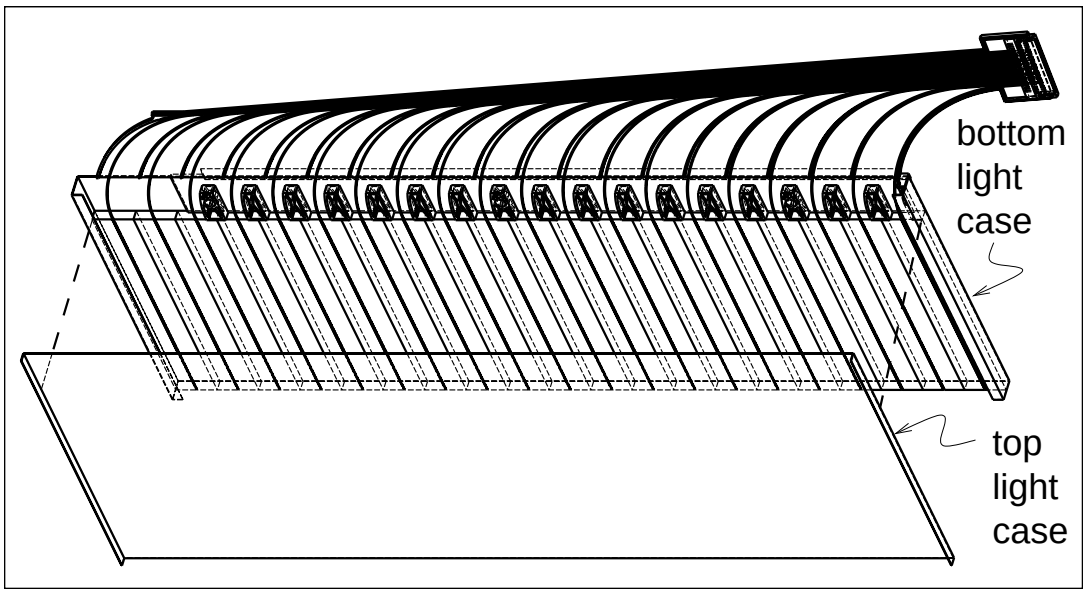

Figure 5.13: Light case assembly, as the top light case is lowered into place onto the bottom light case and strip array, prior to crimping the light case edges.

light cases with scintillator strips in place prior to crimping. The sides of the bottom U channel are bent down 180° to crimp them against the shorter sides of the top U channel. The sides of both the bottom and top U channels are then folded flat against the top of the module.

5.4.3.5 End manifold

The architecture of the end manifolds for perpendicular-ended scintillator modules is described in this Section. These manifolds are functionally identical to those for 45° ended modules. The perpendicular-ended modules have the tightest constraints on fiber bend radius in order to keep the protrusion from the edges of the detector as small as possible. The "snout" design which has been adopted permits all fibers to be routed to one connector while keeping the protrusion from the detector edge as small as possible.

The manifold components of a 20-wide, perpendicular-ended scintillator module are illustrated in Figure 5.14. Optical connectors are mounted on posts on the manifold to join the WLS fibers to the clear-fiber ribbon cables outside the module.

Figure 5.15 shows the detailed design of the end of a 20-wide, perpendicular-ended module. This figure includes the light injection manifold compartment of the optical fiber connector (Section 5.4.3.6), used for strip calibration. Also shown is the mechanical structure (the "integral module mounting bar") which gives rigidity to the manifold and provides a means of attaching the module to brackets on the steel octagon. The bend radii of the WLS fibers are controlled by slots in the base section of the manifold, which guide the fibers into the required paths. The fibers are precut to specific lengths and placed in the slots to produce bend radii of 12 cm, which is the minimum recommended for 1.2 mm diameter Kuraray fibers. All of the end manifold parts are injection molded from optically opaque PVC.

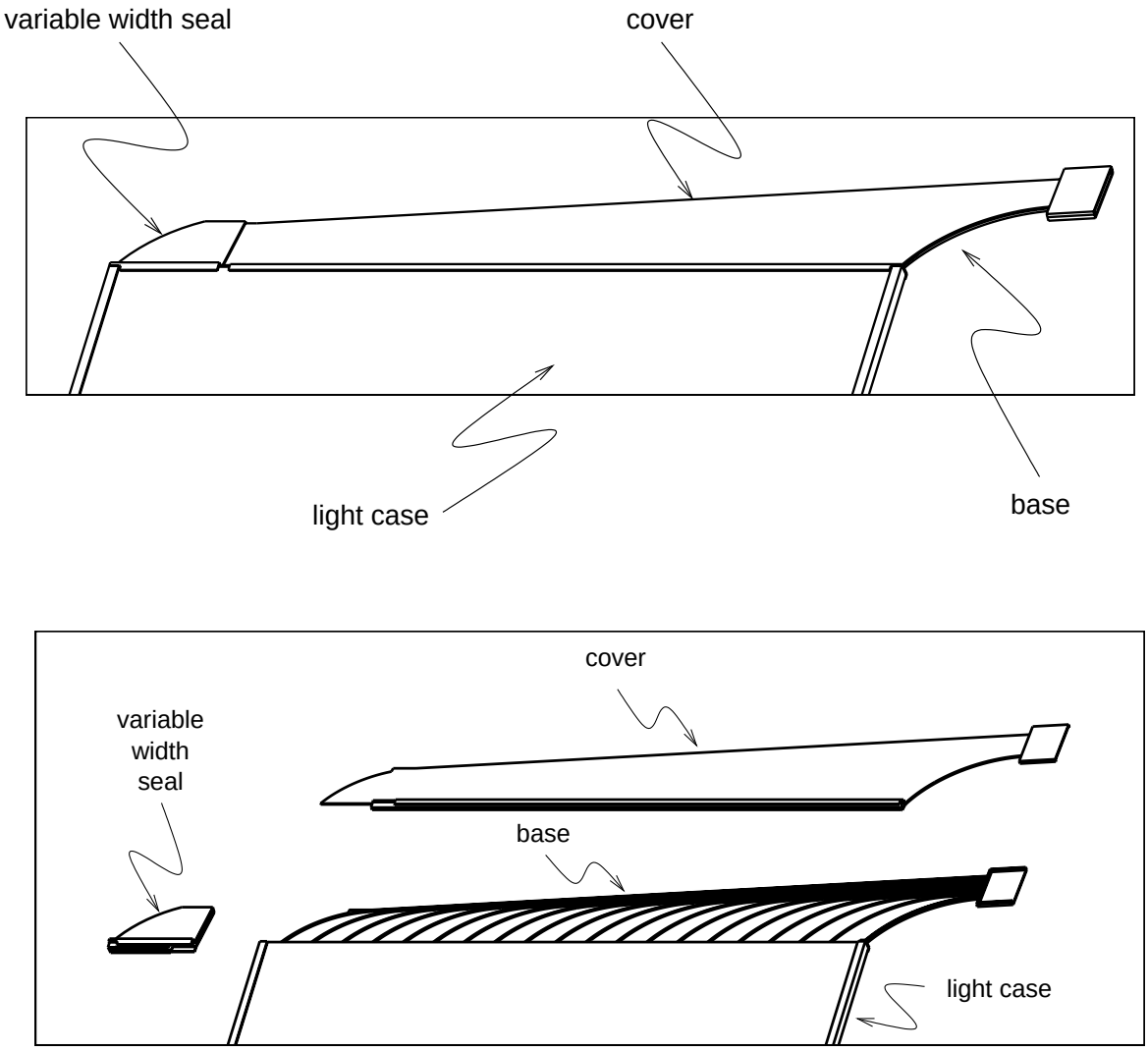

Figure 5.14: Sketches of a 20-wide perpendicular-ended manifold with a right-handed optical connector outlet. The upper drawing shows the assembled manifold and the lower drawing is an exploded view.

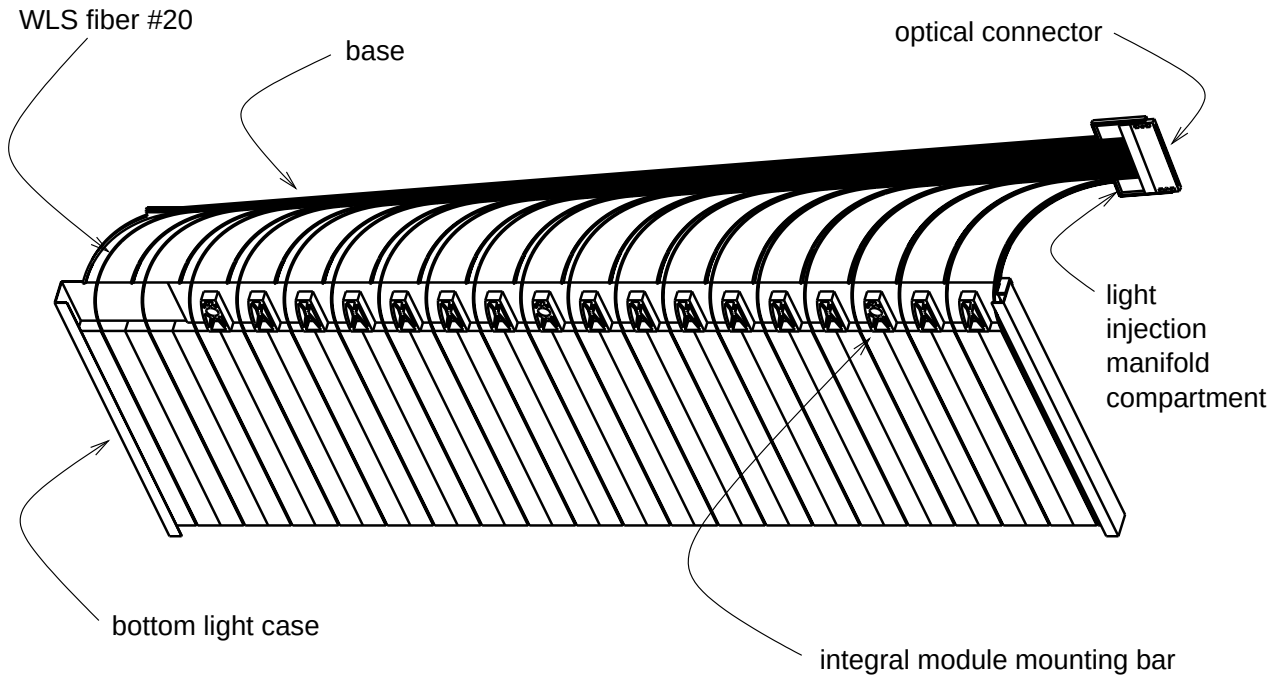

Figure 5.15: Sketch of one end of a partially assembled 20-wide, perpendicular-ended scintillator module, showing the fiber routing and the module mounting bar.

5.4.3.6 Light injection manifold

Light injection manifolds are included in the end manifold assemblies of each module to allow the injection of test pulses of light into groups of WLS fibers. The light injection must be segmented so that only a single fiber will be pulsed on any given PMT pixel at one time (but many pixels can be pulsed simultaneously). This is accomplished by distributing light either to two groups of 10 fibers each for modules which are 20 strips wide, or to three groups of 10, 10 and 8 fibers each for modules which are 28 strips wide. The light injection manifold is an injection-molded block of polystyrene scintillator with 10 parallel grooves on one face and a single hole that enters halfway into the block a few millimeters above the opposite face. Each scintillator module will contain either 2 or 3 of these light injection manifolds depending on the number of scintillator strips contained in the module. Fibers from the laser calibration source are inserted into the holes in each scintillator block, which stop halfway into the block, to illuminate the WLS fibers. The WLS fibers are mounted in the optical connector before they are slipped into the grooves of the light injection manifold. The clear fibers from the laser source distribution system enter each scintillator manifold through a separate optical connector located directly below the optical connector.

5.4.3.7 Module source calibration tube

The source calibration tube assemblies allow small radioactive sources, mounted on piano wire holders, to be moved across the scintillator strips of a module. The tubes are made from 2-mm diameter stainless steel hypodermic tubing and are attached to the aluminum light cases at each end of a module. The tubes are oriented parallel to the strips near the end

manifolds and are curved so that they cross all strips. Each tube is protected by a shield: two pieces of steel wire bent to conform to its shape. The tube and shield are glued to the outside of the light case. The light case is also glued to the scintillator strips in the area underneath the tube to ensure that the tube's position relative to the strips does not change.

5.4.3.8 Coil bypass

A 30-cm wide square hole is provided at the center of each active plane to accommodate the magnet coil. For far detector planes the hole is centered between two perpendicular-ended modules; a semi-circular area is removed from each of these modules. The semi-circular cut extends into the light case and the five scintillator strips at the edge of a module. The WLS fibers for the five cut strips are made long enough so they can be routed around the coil hole.

The semi-circular holes in the affected modules are closed with injection molded plastic bypasses, sealed to the light cases with black adhesive. A bypass is illustrated in Fig. 5.16. The bypass provides a light-tight seal, protects the WLS fibers, maintains the WLS fiber bend radius at more than 12 cm and improves the mechanical integrity of the module in the region of the hole.

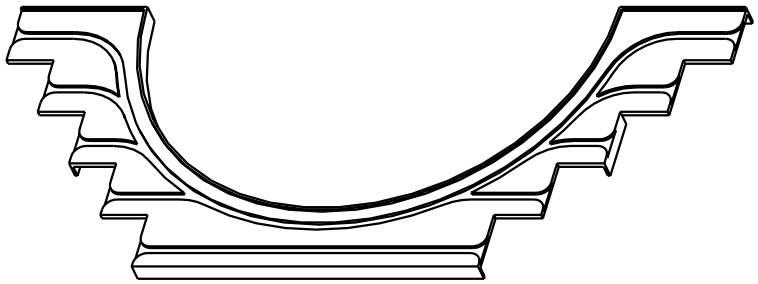

Figure 5.16: Coil bypass.

5.4.3.9 Module mounting hardware

This Section describes the three methods used to attach scintillator modules to the steel detector planes. The actual installation of this hardware is described in Section 7.4.3.2.

The first means of attaching modules to steel detector planes is through the module mounting bars in the end manifolds. Each module mounting bar has a set of holes which penetrate the module and the aluminum light case, as shown in Fig. 5.15. Self tapping screws in these holes are used to attach the both ends of each module to strips of 13 gauge sheet steel which are welded to the edges of the steel detector planes. An elastomeric isolator around the screws cushions the interface between the steel and the modules.

The second means of attachment uses standard 13 mm $\times$ 0.5 mm steel packing straps which wrap around the modules and thread through "switchplate" brackets tack welded to the steel plane. These straps prevent the modules from pulling away from the center

of the absorber planes. Wrapping the straps around two modules at a time minimizes the inter-module gaps.

The third means of attachment is a shelf along the lower 45° edge of each plane mounted on the detector. This shelf supports the lower edge of the bottom module, and the weight of the modules in the plane above it. The shelf ensures that the active planes do not sag in the middle; it does not block access to the optical connectors.

5.4.3.10 Differences in near detector modules

The scintillator modules in the near detector share all of the essential features of the far detector. However differences in the size and functional regions of the near detector result in some differences in module construction and layout:

- The modules for the fully instrumented planes, e.g., in the muon-spectrometer section, are similar to those of the far detector except that they are at most 4 m in length and are read out from only one end. Modules in the muon spectrometer section have 4-fold multiplexing to the photodetectors instead of the 8-fold multiplexing used for the far detector.

- The modules in the partially instrumented planes of the target/calorimeter sections are less than 2.7 m long and are also read out from only one end. None of the modules in these forward sections have multiplexed readout, i.e., they have only one fiber per photodetector pixel.

- In order to keep the calorimetric response between the near and far detectors as similar as possible, we plan to modify the design of the near detector modules slightly so that the calorimeter section of the near detector has a one-ended light yield very close to that of the sum of two ends in the far detector. To first order, this occurs naturally since WLS fibers in the near detector are shorter than those in the far detector. However, it may be desirable to include a crude mirror on WLS fibers in the near detector (e.g., white paint on the fiber ends) or to use slightly larger diameter fiber in order to make the best match between the near and far detector light outputs. This will also ensure good efficiency for muons from the spectrometer section of the near detector.

5.4.4 Photodetectors (WBS 2.2.4)

5.4.4.1 Photodetector requirements

MINOS neutrino events produce a wide range of light levels in the scintillator strips. On the low end, muons give at least 1.7 photoelectrons from the lower of a strip's two readout ends (at least 5.5 photoelectrons from the sum of the two ends), and the tails of showers range down to single photoelectrons. On the high end, we want to maintain linear response for showering events with up to 500 photoelectrons per strip on a single pixel. MINOS photodetectors must meet this and other specifications:

1. Linearity over a physics dynamic range of 500.

2. Ability to discriminate at 1/3 of a pe level with acceptably low noise.

3. Shaping times $< 1\mu$s to avoid pile-up at the near detector.

4. Dark count below 10 Hz/mm^2 of photocathode area.

5. Lifetime of 1 to 3 mC integrated charge and a failure rate of less than 2% per year of operation.

6. Less than 10% effect on gain for up to 10 Gauss magnetic fields.

7. Crosstalk between neighboring pixels $< 4\%$.

8. Quantum efficiency $\times$ collection efficiency such that a muon crossing a strip gives at least 2.5 total pe's observed on average.

9. Pixel-to-pixel nonuniformity of 4:1 or better. Nonuniformity increases the electronics dynamic range requirement.

10. Time resolution of better than 2 ns for signals of >10 pe's.

These requirements are met by several commercially available photodetectors, of which multi-pixel photomultipliers are the most attractive for MINOS. We have chosen the Hamamatsu R5900U-00-M16 16-pixel photomultiplier for the MINOS baseline design because of the extensive favorable experience of other experiments with this photodetector.

5.4.4.2 Baseline photodetector

The baseline photodetector for MINOS is a 16-pixel, multi-anode photomultiplier, R5900U-00-M16, manufactured by Hamamatsu Photonics[14]. Our choice of the 16-anode M16 is based on two simple criteria: a) R5900U-00-M16 satisfies all our requirements, and b) among all multi-anode photomultipliers it provides the lowest cost per unit area of the photocathode. The M16 tube behaves like 16 miniature single-channel phototubes. Only a few additional and potentially adverse features, like cross-talk and nonuniformity of pixel response, are introduced through dense packaging. Figure 5.17 and Table 5.2 show the geometry and basic characteristics of the M16. The R5900 family of multi-anode photomultipliers includes tubes with numbers of channels ranging from 1 to 64, with independent anodes and metal-channel dynode structures. Hamamatsu maintains an active R&D program to improve performance of the R5900 series of tubes. The most recent example of this effort is development of an improved bialkali photocathode for the M16 tubes, which gives about a 10% increase in quantum efficiency over previously produced bialkali photocathodes.

The R5900U-00-M16 tube has a wide range of applications. It is used in biomedical imaging as well as in major high energy physics experiments. The HERA-B detector at DESY uses 1500 of these tubes in the central part of the ring-imaging Cerenkov counter readout[15]. The upgraded Plug of the CDF II detector at Fermilab employs about 450 tubes in the readout of the Preshower and Shower Maximum detectors[16].

Several high energy physics groups, including MINOS, have conducted many comprehensive tests on the M16 tubes during the last year[17]. These studies have provided valuable

Parameter	Description/Value
Photocathode material	bialkali
Window material	borosilicate glass
Window thickness	1 mm
Spectral response	300 to 650 nm
Wavelength of maximum quantum efficiency	420 nm
Quantum efficiency at 520 nm	13 %
Dynode type	metal channel structure
Number of stages	12
Anode	an array of 4×4 independent pixels
Anode dark current per channel	≤ 1 nA
Pixel size	4 mm $\times$ 4 mm square
Maximum high voltage	1000 V
Gain at maximum HV	3.9×10^7
Nominal operating gain for MINOS	10^6
Anode pulse rise time	0.83 ns
Transit time spread per channel (FWHM)	0.3 ns
Pulse linearity per channel ($\pm$ 2 % deviation)	0.5 mA
Cross-talk (4×4 mm^2 aperture)	1 %
Pixel-to-pixel gain variation	1:4

Table 5.2: Basic characteristics of the R5900U-00-M16 16-channel photomultiplier produced by Hamamatsu Photonics.

practical experience and allow us to project with high confidence the performance of mass-produced M16 phototubes. Also, the delivery capacity and reliability of the manufacturer is now well established. In this Section we briefly discuss selected features of the M16 tube which are relevant for the MINOS scintillator detector and associated electronics.

- **Quantum efficiency:** The expected light yield for minimum ionizing particles requires that a photodetector be able to clearly separate single photoelectron signals from the pedestal. Since the emission spectrum of the wavelength shifting fibers peaks at about 500 nm, and is further shifted to about 520 nm due to length attenuation, we require high quantum efficiency for photons with wavelengths of about 520 nm.

  Figure 5.18 shows a typical distribution of pulse heights obtained by pulsing a wavelength shifting fiber with a blue LED. Peaks of 1, 2, and 3 photoelectrons can be easily identified. The new M16 tubes have an improved bialkali photocathode with a typical quantum efficiency of about 13% at 520 nm, as shown in Figure 5.19. This constitutes a $\sim$10% improvement over older tubes of this type.

- **Pixel-to-pixel response uniformity:** Studies by Hamamatsu, HERA-B, and MINOS show that individual pixels of the M16 tube can produce significantly different anode

pulse heights for the same illumination. Figure 5.20 presents an example of response uniformity for one M16 tube. The gain of the inner pixels is typically lower than the gain of the perimeter pixels. About 30% of channels are currently expected to exceed a maximum to minimum response ratio of 2.5. This nonuniformity has no serious adverse effects for MINOS. Its main impact is the increase of the dynamic range requirement on the front-end electronics. For MINOS, Hamamatsu guarantees the ratio to be less than 4.

- **Pixel response uniformity:** Eight 1.2 mm diameter fibers will be multiplexed onto one 4×4 mm^2 pixel. Although there are variations in intra-pixel collection efficiency, our measurements show that these are almost completely averaged out for 1.2 mm diameter fibers. Some pixels have intra-pixel variations in gain for 1.2 mm diameter fibers which are comparable to the inter-pixel gain variations. These intra-pixel gain variations can be directly measured for each fiber using our calibration system, and have the same effects as the inter-pixel gain variations.

- **Fast timing:** We have measured the time resolution of the Hamamatsu M16 tube to be better than 2 ns for greater than 10 observed pe's. Figure 5.21 shows the measured time resolution for the Hamamatsu M16 tube as a function of the number of observed photoelectrons. For these small numbers of pe's, the time resolution is dominated by the decay time of the Y11 fluor in the WLS fiber rather than measurement effects in these photodetectors. This time-of-flight measurement capability will be useful in determining the direction of showering events induced in the MINOS far detector by cosmic-ray neutrinos, and is better than required for determining the direction of high-energy muons traversing the detector.

- **Magnetic field sensitivity:** The M16 tube is a proximity focused photomultiplier with an additional electron focusing grid placed before the first dynode. This architecture assures relatively low sensitivity to magnetic fields. In locations on the MINOS detector in which photodetectors will be installed the expected magnitude of the fringe magnetic field is about 7 Gauss. Unshielded M16 tubes could typically lose about 5 to 10% gain in such a field. However, magnetic fringe fields could have a more serious effect on cross talk between neighboring pixels, particularly for fibers located near pixel edges. To eliminate this effect, a thin soft iron sleeve (2 mm thick transformer laminate) surrounds each MUX box, reducing the field at the photodetector by a factor of five or more.

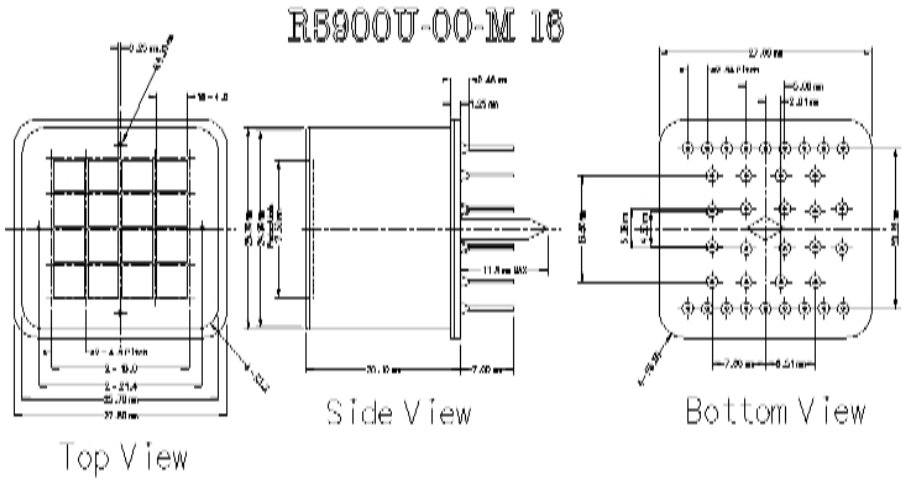

Figure 5.17: Detail drawing of the Hamamatsu R5900U-00-M16 multi-anode photomultiplier.

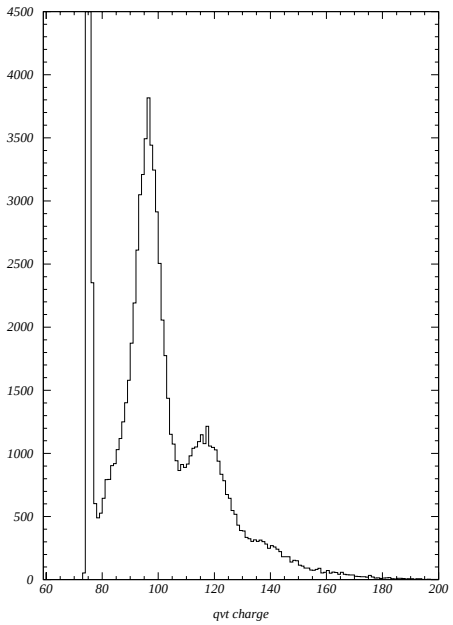

Figure 5.18: A typical pulse height distribution in a pixel of an M16 tube obtained by pulsing a wavelength shifting fiber with a blue LED. Peaks for 1, 2, and 3 photoelectrons are clearly visible.

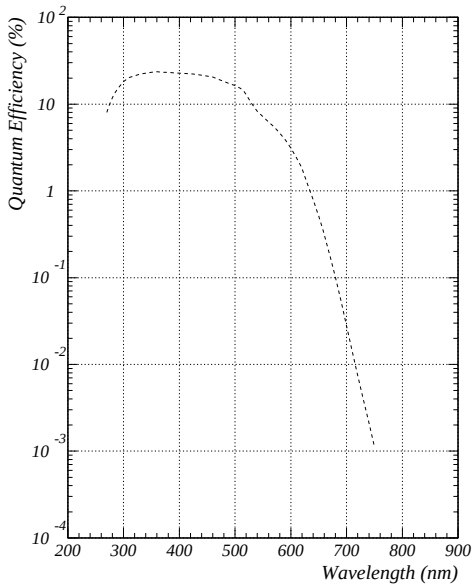

Figure 5.19: A typical spectral response for a Hamamatsu R5900U-00-M16 tube. For MINOS the most important wavelengths are at about 520 nm, the maximum of the emission spectrum of the wavelength shifting fiber.

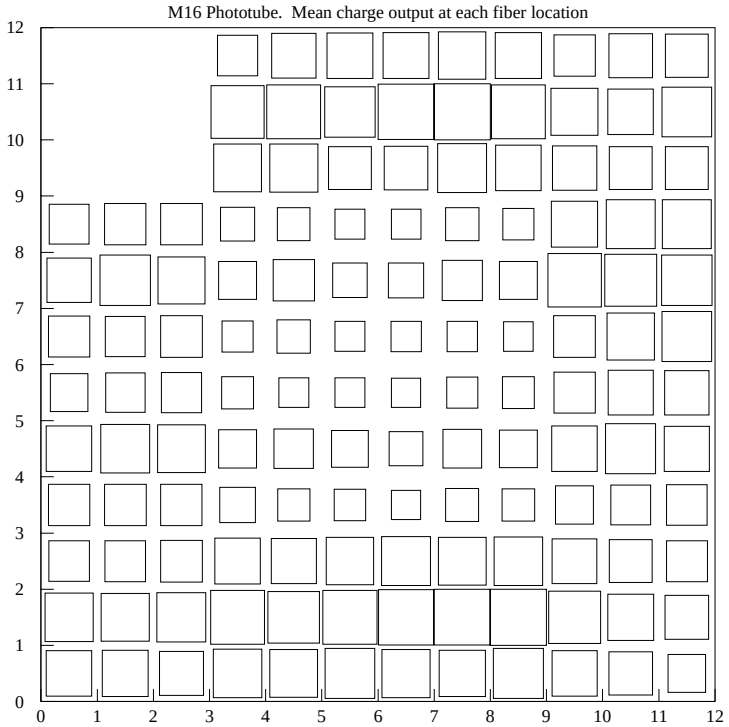

Figure 5.20: A typical response of an M16 phototube. Each pixel was illuminated using a 1 mm diameter wavelength shifting fiber with the same amount of light. On each pixel the fiber was placed in 9 locations in a 3×3 grid. The area of the squares in the plot are proportional to the signal on the anode. A pixel-to-pixel response nonuniformity, and variation within one pixel, are clearly visible. The measurement showed that the observed structure can be attributed mainly to the variation of the effective gain in individual channels rather than quantum efficiency or collection efficiency. One corner pixel was not read out.

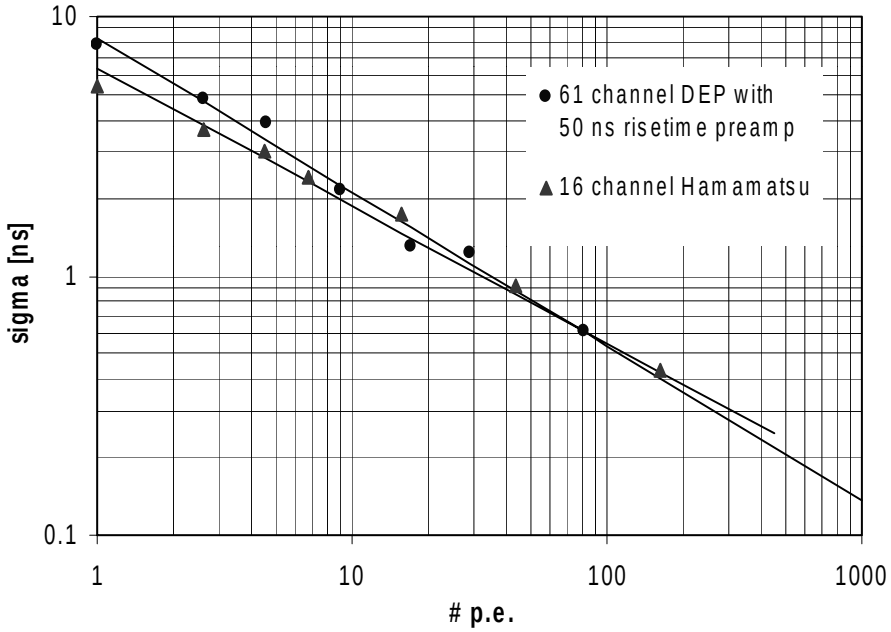

Figure 5.21: Time resolution (σ) measured as a function of the number of observed photoelectrons for the Hamamatsu M16 and DEP HPD reading out WLS fiber. The resolution for small numbers of pe's is dominated by the decay time of the Y11 fluor in the WLS fibers. Of particular interest is the better than 2 ns σ for more than 10 observed pe's which will be useful in determining the direction of showering events.

5.4.5 Connectors and multiplexing boxes (WBS 2.2.5)

5.4.5.1 Fiber connectors

Construction of a modular detector requires efficient and cost-effective fiber-to-fiber connectors. In MINOS, optical fiber connectors are used to couple the WLS fibers coming from the scintillator modules to the clear-fiber ribbon cables and between the ribbon cables and the multiplexer boxes. Such connectors have already been developed for the CDF endplug upgrade (10 fibers), the D0 upgrade (about 100 fibers), and recently for the CMS HCAL (18 fibers). Tests on these connectors have shown similar performance in light transmission. For MINOS, we are planning a custom-designed connector based on one of the previous designs. The MINOS connector will be a 28-wide connector with 2.3 mm pitch for the fibers. (This is most similar to the CMS connector which is 18 wide and with 2.3 mm fiber pitch.) The reason for designing a custom connector rather than just using one of the existing connector designs is cost. To a good approximation, the cost per connector and manpower to assemble it is the same regardless of the design or the number of fibers included (up to some reasonable limit). Furthermore, the cost of clear fiber ribbon cables is much lower if a pitch of about 2 mm is used rather than a pitch of about 1 mm as for previous cables. We are currently evaluating the different connector designs to decide which is optimal for MINOS

needs. We have used both 10-wide CDF connectors and prototype CMS-style connectors in construction of MINOS prototype modules. We find similar results for light transmission from the two types of connectors.

A sketch of a MINOS connector at a 20-wide scintillator module manifold is shown in Figure 5.22. The connector is wide enough to accommodate 28 optical fibers in order to allow just one connector design for all modules. The 8 unused fiber positions are plugged when the connectors are used for 20-wide modules. Appropriately matched connectors are located on the scintillator manifolds, the MUX boxes and each end of clear fiber ribbon cables which connect the two. MINOS ribbon cables are 10 and 8 fibers wide (these are already a custom production so there is no problem specifying these widths). Fibers are glued into the connector housing with epoxy, with a few mm of the fiber left protruding. The protruding fibers are fly cut and polished using a diamond fly cutter. Prototype 28-wide connectors are currently being produced for MINOS.

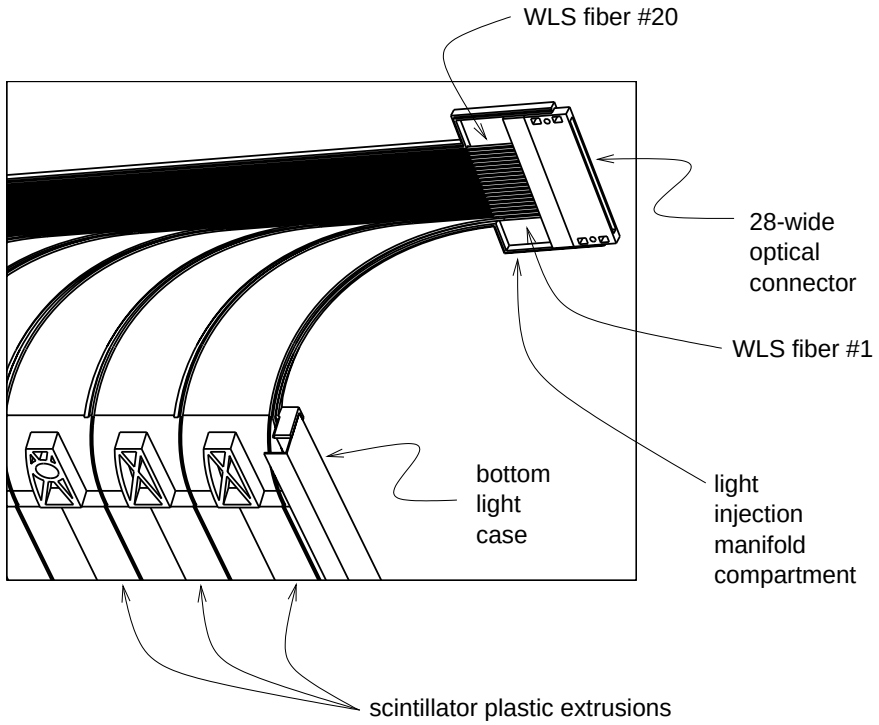

Figure 5.22: Sketch of a MINOS 28-wide optical connector for 1.2 mm diameter fibers, as used on the end manifold of a 20-wide scintillator module.

The CDF connectors were manufactured by the DDK company of Japan[18]. CDF has measured the light transmission across the connector without optical coupling. The mean of the measured light transmission is 83%[10] with small spread. Out of the total light loss of 17%, 10% is expected from the Fresnel reflection. The light loss can be reduced by using optical couplant. The DO collaboration has measured an average light transmission of 90$\pm$5% using a diffused light source and 96$\pm$3% using a small angle light source[13] for their tracker and preshower detector for the upgrade, but with use of an optical couplant.

CDF has measured the reproducibility of the light transmission for this connector through multiple repetitions of disconnecting and reconnecting. The rms width of the distribution is less than 2%[10]. Our first test results show that MINOS connectors will provide similar performance.

5.4.5.2 Multiplexing boxes

The multiplexing (MUX) box is the link in the readout chain between the signal fibers and the photomultiplier tubes, as shown schematically in Figure 5.4. The mechanical structure of the MUX box is shown in Fig. 5.23. The input signals from the detector are brought to the MUX box by clear optical fibers, bundled into ribbon cables, that plug into bulkhead connectors on the front plate. Inside the MUX box, clear fibers are mated to the signal fibers and then routed to the back plate through an aluminum box chassis. At the back plate, the fibers are laced to three internally mounted cookies that are machined to align precisely with the pixels of three 16-channel PMTs. The MUX box is designed to be light tight and is shielded against magnetic fringe fields.

External to the MUX box on the back plate, the cookies are mated to the PMTs by means of a PMT-cookie assembly. This assembly, shown in Fig. 5.24, allows for the removal/replacement of a PMT without opening the MUX box. In this design, the cookie remains in a fixed position with respect to the cookie holder. To allow for tolerances in the manufacture of its case, the PMT is cemented into an outer jacket. This jacket fits precisely into a holder that permits piston-like motion with respect to the cookie but very little lateral motion. The piston-like motion enables the spring-loaded PMT base to push this assembly into contact with the cookie. The precision alignment of the cookie with the PMT is accomplished by aligning the cookie holder with the PMT holder using a special alignment tool; the alignment procedure takes place in the lab, away from the detector.

The three PMT-cookie assemblies are bolted to the back plate and housed in a light-tight PMT cover box. The electronics are connected to the PMT outputs through the PMT cover box.

There are 484 MUX boxes in the MINOS far detector. The far detector makes use of 8$\times$ multiplexing on the PMT pixels while the near detector will make use of 4$\times$ multiplexing in the muon spectrometer section and no multiplexing in the target/calorimeter section. However, the same design for both the MUX box and electronics will be used for the near detector. Near detector MUX boxes have fewer connectors on their front plates, fewer fibers to be routed, and special cookies to accommodate the particular number of fibers in each type of box. There are a total of 212 MUX boxes in the near detector.

- **Mechanical construction of the MUX box**

  All MUX box components shown in Fig. 5.23 are stamped and formed from sheet aluminum. The boxes are assembled with stainless steel self-tapping sheet metal screws. Each box is surrounded by a 2 mm thick sleeve of soft iron transformer laminate to shield the photodetectors against magnetic fringe fields (not shown in Fig. 5.23).

  The inputs to each MUX box are 1.2 mm diameter clear polystyrene fibers carrying the signals from two consecutive detector planes with the same stereo view. These 384 signal fibers are bundled in ribbon cables. Each of these ribbon cables terminates in

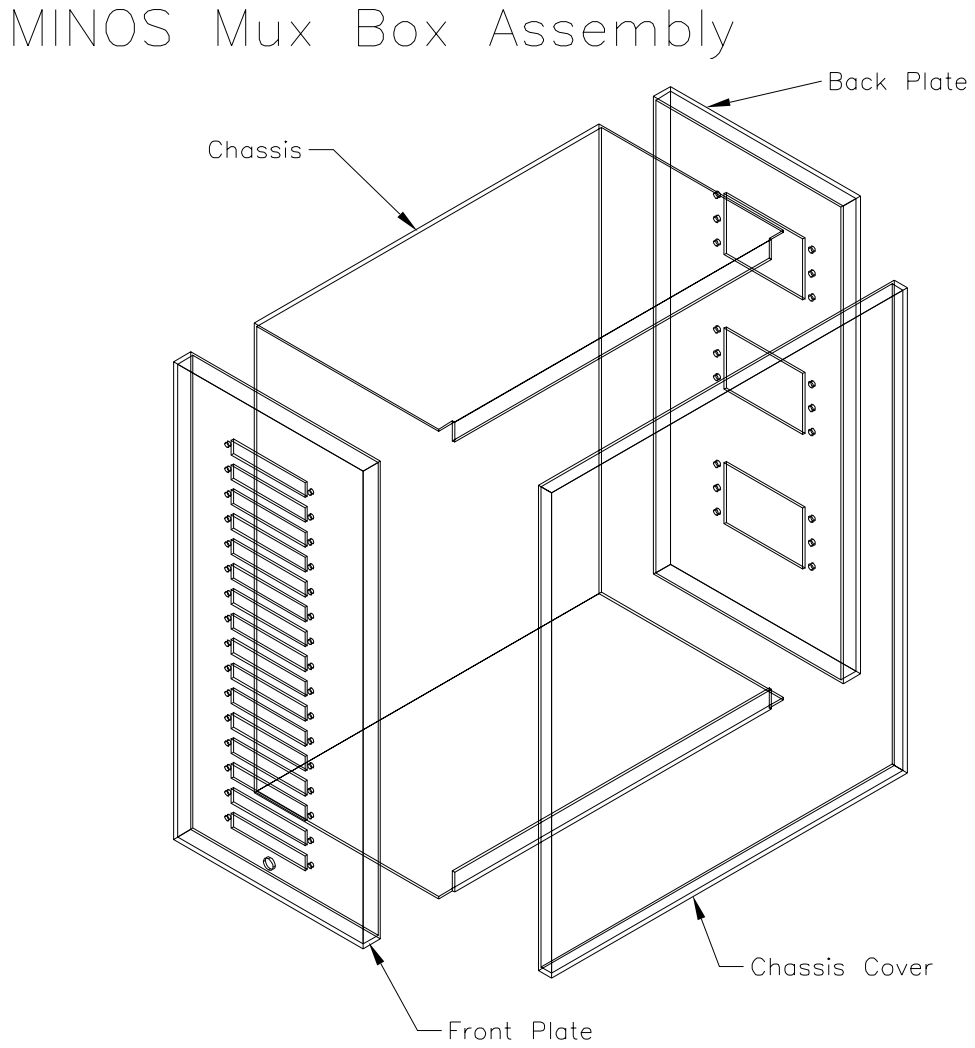

Figure 5.23: MUX box assembly. The external magnetic shield of 2 mm thick soft iron which surrounds the box is not shown.

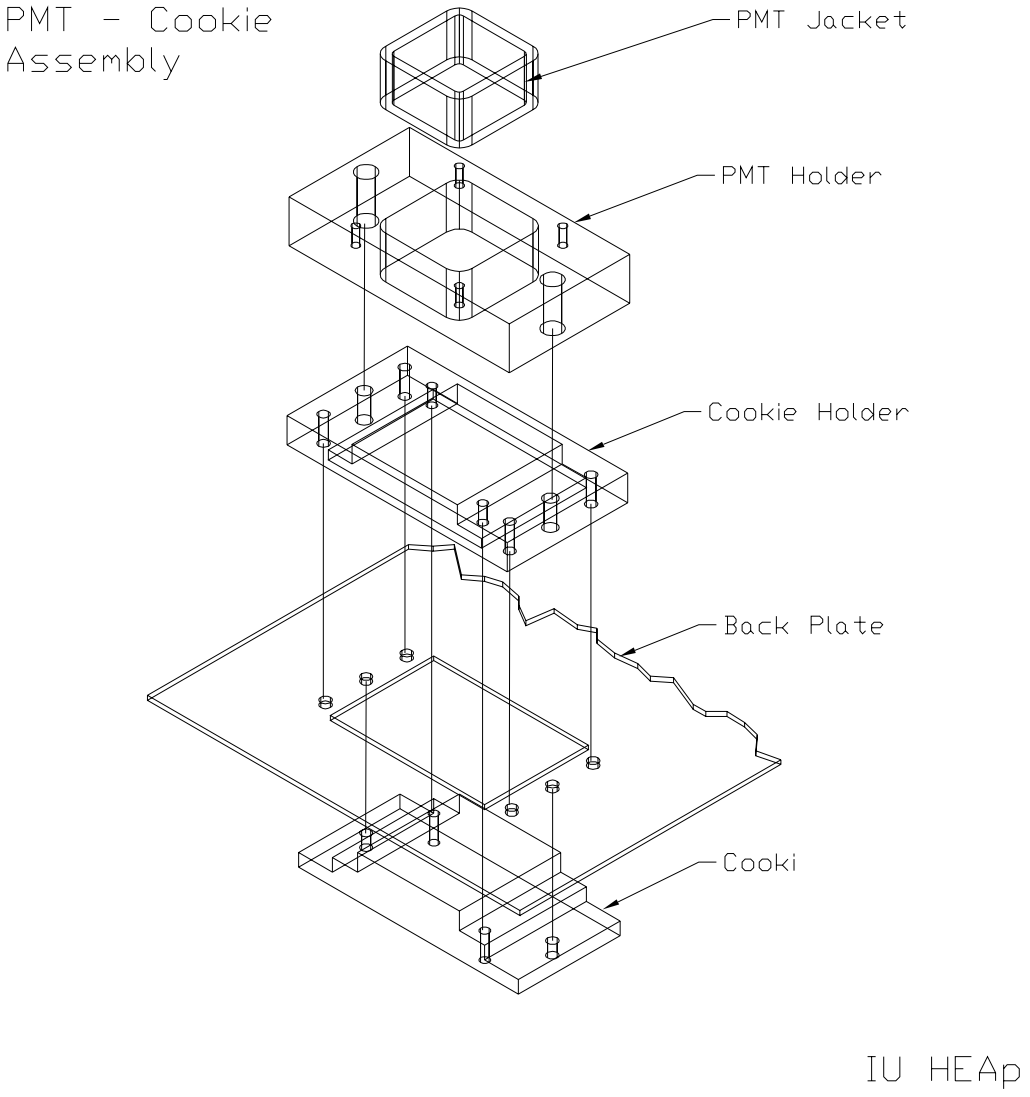

Figure 5.24: PMT-cookie assembly.

a fiber optics connector (see Section 5.4.5.1) that plugs into a double female bulkhead connector mounted on the MUX box front plate. Inside the MUX box, groups of eight clear fibers mate to the signal fibers through the front plate bulkhead connectors. A hole is provided near the bottom of the front plate to mount an LED and diffuser on the inside of the MUX box, as described in Section 5.4.6.2. The internal signal fibers are routed from the front plate, through the box chassis, to the cookie on the back plate. The 25-cm length of the MUX box chassis is set by the requirement that the bend radius of the fibers be greater than 12 cm.

- **Routing and fly cutting fibers**

  The 384 signal fibers are routed to three Hamamatsu M16 multichannel PMTs through precision-machined cookies. Eight fibers are routed to each 4 mm $\times$ 4 mm pixel. Two of the PMTs in a far-detector MUX box see $8 \times 16 = 128$ fibers from single planes; the third PMT sees $8 \times 8 = 64$ fibers from each plane. The ribbon cable connectors are inserted into the front plate according to a pattern that minimizes fiber lengths within the MUX box.

  The baseline detector has 8-fold multiplexing and 2-ended readout. To resolve ambiguities introduced by the multiplexing, the two strip readout ends will have different routing/lacing schemes. On a single pixel, fibers arrive from each of the eight logical modules within a scintillator plane. The exact scintillator strip location (within the logical module) to pixel location map is permuted within groups of eight fibers. Monte Carlo simulations of neutrino events show that this mapping permits unambiguous identification of the true location of neutrino events for light levels meeting our specifications.

  For cookie assembly, the fibers are first glued into the connectors. Then the connectors for a group of 128 fibers are fixed to a jig and the fibers routed to the cookie according to the appropriate permutation scheme. To facilitate accurate routing to a particular cookie position, the fibers are illuminated with the same programmable LED sources used for quality control checks (see the final bullet in this Section). After gluing the connectors and cookie are fly cut with a commercial fly cutting machine. The procedure for inserting the fibers into the connectors and then lacing the cookie was developed for CDF. However, for MINOS the procedure for routing the fibers to the appropriate cookie hole is more complicated than for CDF. We have begun to optimize this procedure by actual prototype assembly in order to estimate the manpower required.

- **PMT-cookie assembly**

  The PMT-cookie assembly is shown in Fig. 5.24. The cookie is injection molded from grey Noryl and mounted inside the MUX box on the back plate. It has 16 precision holes that accommodate 1.2 mm fibers in a 3-2-3 pattern (three fibers on top and bottom with two fibers in between, arranged in a close-pack array). The cookie holes precisely align with the 16 pixels on the PMT. The cookie mates with a cookie holder outside the MUX box. The cookie holder has a central hole with the exact shape of the cookie and is attached to a PMT holder using slightly over-sized holes. These holes

allow the cookie to be accurately aligned with the pixels on each individual PMT. This alignment is done in the lab using a special clear acrylic 'alignment cookie' with the exact shape of an actual cookie. Both the cookie and the alignment cookie have sockets for two alignment dowels that rigidly fix the cookie and the alignment cookie in the same position relative to the cookie holder to within tolerances of a few thousandths of an inch. The alignment cookie has precision ruled marks that accurately line up with the guide marks on the PMT photocathode. The cookie holder with the alignment cookie is accurately aligned with the PMT holder before they are rigidly fixed to one another.

The PMT is pressed against the cookie, piston-like, by a spring-loaded base. The PMT is glued into an aluminum jacket that allows for the 0.5 mm tolerances on the PMT housing. The outside of the jacket is precisely machined to fit into the PMT holder in a way that allows it to slide without lateral motion. The PMT base is attached to the PMT holder. The cookie holder, PMT holder, PMT, and base assembly are then attached to the cookie. A light-tight housing is placed over the PMT-cookie assembly and bolted to the back plate.

- **QC computer controlled LED array**

  Final checkout of the lacing scheme and the MUX box will be made using a programmable set of LED sources. A set of pattern-generation LED boards is driven by a computer. Clear fibers from the LEDs run to optical connectors which couple to the MUX box connectors. To test the lacing pattern on a cookie: (a) each of the lacing schemes is programmed into the computer; (b) individual fibers are illuminated in such a way that only one fiber in each of the 16 pixel holes on the cookie lights up; simple pattern recognition is performed by eye; (c) the test is then repeated 8 times for each cookie. The completed MUX box will be tested with this computer controlled LED array by flashing attenuated LED signals through each fiber and measuring the PMT output.

  This testing device is also used to facilitate fiber lacing. For this task, the QC computer is programmed to illuminate the 8 fibers that are to be routed from the connectors to a particular pixel hole on the cookie. By plugging and gluing only lighted fibers, fiber routing becomes simpler, more accurate, and less time consuming.

5.4.5.3 PMT bases and mounting

The M16 photomultiplier and its mounting brackets are rigidly attached to the back plate of the MUX box. A square opening in the plate lets the fibers couple to to the photocathode face. The tube is aligned with fibers as described in the preceding Section. The PMT base (voltage divider board) is mounted directly on the pins of the tube. For strain relief this board is also attached to the PMT holder using 4 spacer screws placed in the corners of the board. The entire phototube assembly (i.e., a cookie, a cookie holder, PMT holder, PMT, and the voltage divider card) is housed in a light-tight case sealed to the back plate of the MUX box.

A multi-purpose feed-through D-type connector on the PMT housing supplies HV to the photomultiplier and also carries 16 anode and one common dynode signals. The three

PMT connectors on the MUX box are aligned to mate directly with connectors on the front-end electronics card. The PMT base provides a negative high voltage bias for the dynode structure and also routes the anode signals. "Tapered" resistor values allow a gain of about 10^7, up to 5 mA anode current, and response linearity of $\pm 2\%$ over the entire range of physics and calibration pulses. Heat generated by the divider current (0.4 W for 250 μA at the maximum high voltage of 1000 V) is easily dissipated by the PMT mounting structure and the multiplexing box. This arrangement mechanically decouples the front-end electronics board from the photomultiplier and at the same time provides a short signal path and good noise shielding.

5.4.6 Calibration systems (WBS 2.2.6)

The calibration system provides the means of understanding the calorimetric response of the near and far detector for hadrons and electrons and ensuring that the relative response between the two sites is understood. The goal is to calibrate the hadronic energy response to an absolute level of 5% and a relative level of 2% between the near and far detectors. This requires several different calibration systems as described in the following Sections. Cosmic-ray muons provide an integral part of the system. The calibration plan is discussed in Section 5.4.6.6.

5.4.6.1 Laser light distribution

The baseline design for the MINOS light injection system uses UV laser light sources. The laser light illuminates scintillator blocks surrounding sets of eight or ten WLS fibers. This ensures a good match between the spectrum of light from the calibration system and the scintillation light from real neutrino events. The advantages of a laser system are:

- The laser pulses are extremely short (<5 ns) so that the time profile of the pulse reaching the PMT is dominated by the WLS dyes. This makes calibration pulses very similar to those from a particle.
- Optical filters are used to attenuate the light at well-controlled predefined values.
- With one laser it is possible to illuminate $\approx$ 5000 WLS fibers at once, so only a small number of lasers is needed.

The far detector requires a single laser coupled to an optical fiber routing network which is used to inject light into the light injection manifolds described earlier. The pulses from the laser can be directed under computer control to distribution points located at the corners of each supermodule as shown in Figure 5.25. The placement of the components is designed to minimize the lengths of fiber in the system. Figure 5.26 shows a schematic for the distribution network. The laser which pulses the system is a N_2 laser which can deliver several hundred micro-joules per pulse at a wavelength of 337 nm. Each laser feeds a distribution system of splitters and fibers allowing it to pulse 1/20 (i.e., one physical light injector module per plane) of each detector block in a given view at a time. This results in only one fiber at a time being pulsed on each photodetector pixel. The laser is equipped with a computer

controlled attenuation wheel, containing neutral density filters, to provide a wide dynamic range for test calibration. A gain-stabilized reference photodetector monitors pulse to pulse variations of the laser output. To ensure the stability of the monitor photodetector, it also views a NaI(Tl) crystal with an imbedded ^{241}Am source. The laser light is transported to the fanouts by quartz fibers, and between the fanouts and the scintillator modules by acrylic fibers. This provides acceptable attenuation at reasonable cost.

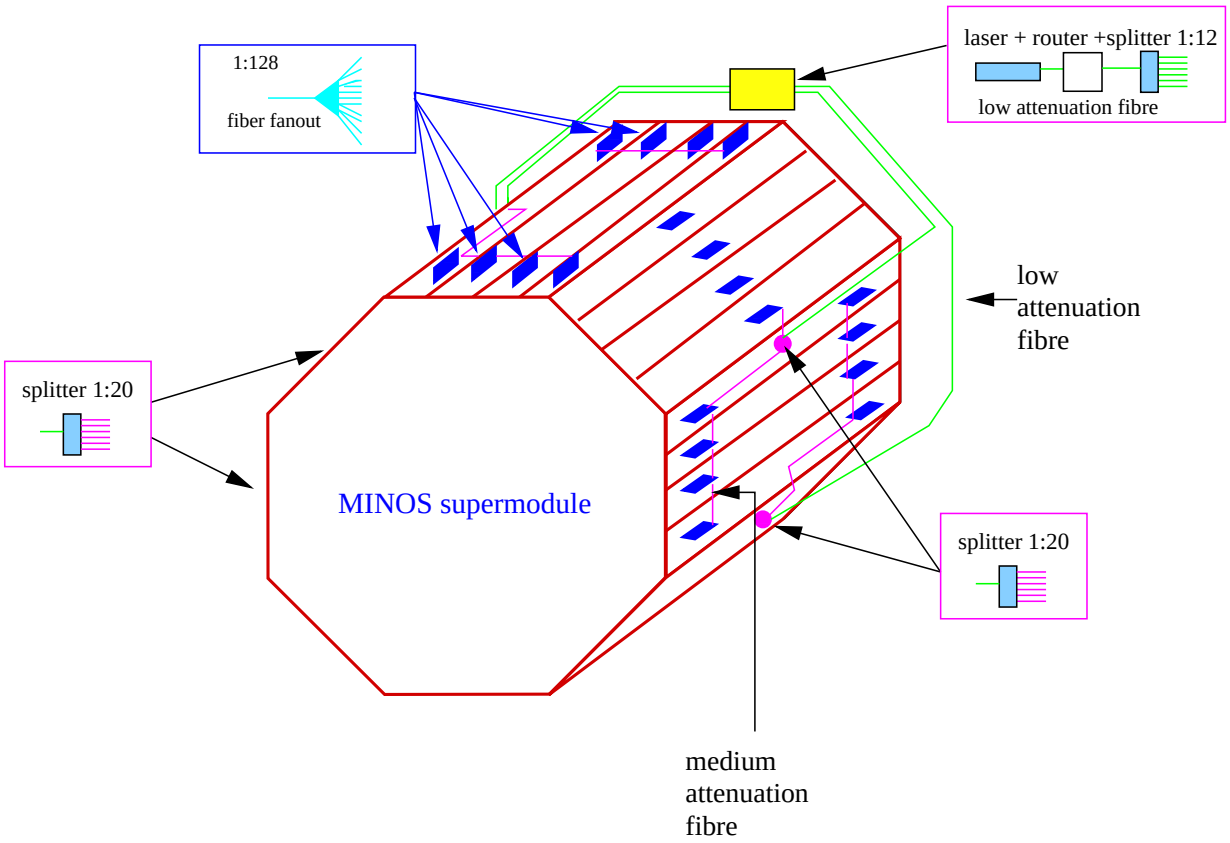

Figure 5.25: Location of components for the laser calibration system.

A similar light-injection system is being implemented as part of the CDF plug upgrade[16]. The CDF laser produces approximately 4.7×10^{14} photons per pulse. The overall light delivery efficiency of the CDF system is $\approx 1.3 \times 10^{-8}$. (This includes coupling to the fiber from the laser, light loss in transmission, light loss in the primary distribution to the splitter boxes, loss of light inside the splitter boxes, laser light dumped in a scintillator block, scintillation light coupling to WLS fibers, and light coupling to the PMTs.) In the system we are planning, we have essentially the same set of steps in our light delivery system except for the losses of light due to transmission in acrylic fibers instead of glass fibers. Both CDF and MINOS use the same Hamamatsu PMT. In CDF, there are 6.2×10^6 photons reaching the photocathodes through approximately 1000 fibers. Folding in a 10% QE in the PMT and dividing out the fiber count, results in 6.2×10^2 pe's per fiber, which will be enough light for the high energy end of the calibration.

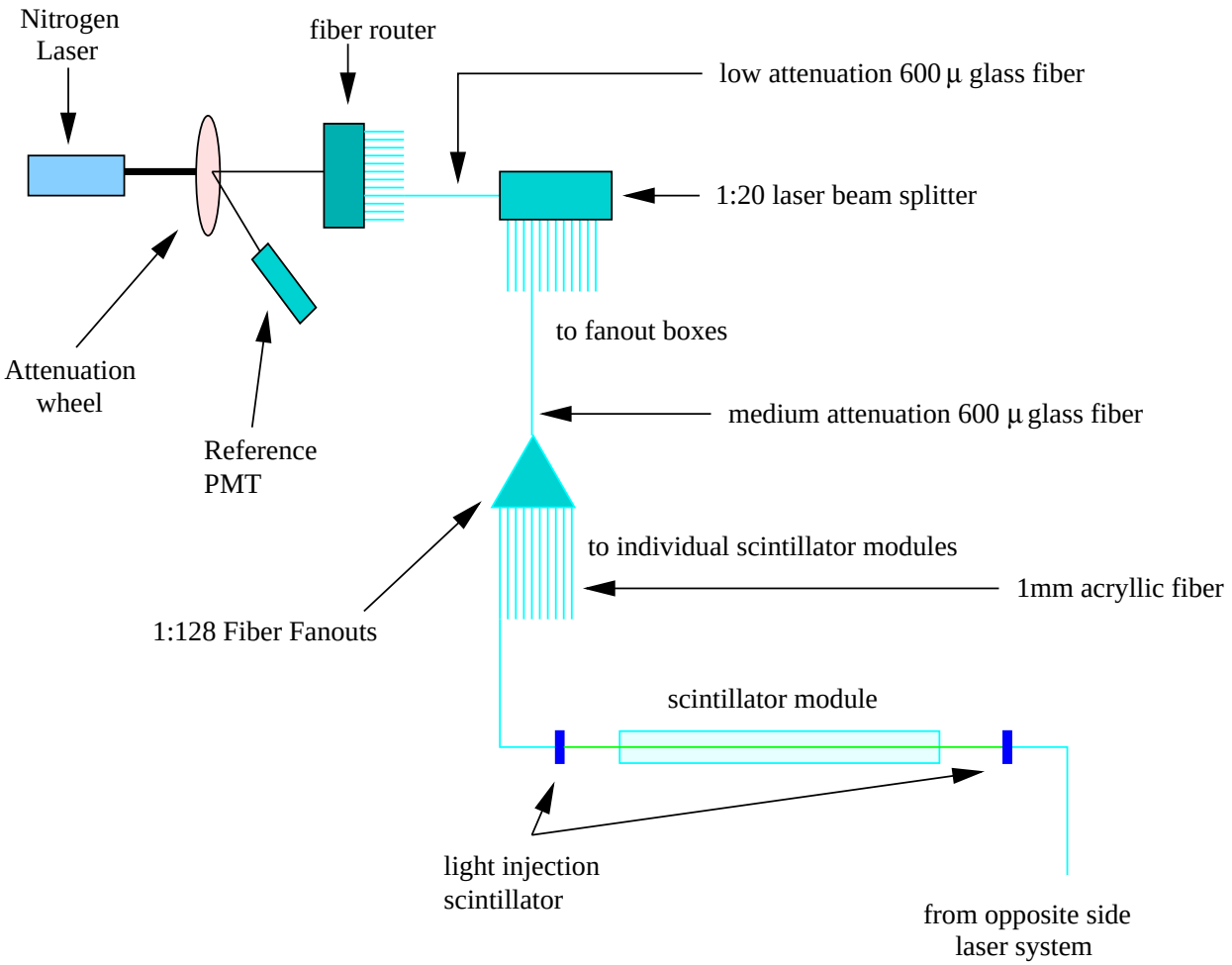

Figure 5.26: Schematic of the distribution network for the laser calibration system.

It is not necessary to have complete uniformity in the light injection system as long as the illumination is constant over time. Differences in intensity of up to 30% are acceptable across the WLS fibers within a manifold. Differences of up to a factor of two are acceptable for the amount of light arriving at completely different photodetectors. (More light settings are then required to get a complete calibration.)

5.4.6.2 Light injection to photodetectors

A green (505 nm) ultra-bright LED is installed in each MUX box to help isolate light transmission problems in the readout chain. The LED is pulsed at a low voltage level to check the response from all pixels of the three photodetectors simultaneously.

5.4.6.3 Radioactive source system

The purpose of the source system is to obtain a rapid measure of the response of each scintillator in the detector. Short stainless steel tubes are attached at either end of a detector module as described in Section 5.4.3.7. A tube acts as a guide track for a 3 mC ^{137}Cs source attached to the end of a piano wire. The source position is controlled by a drive mechanism under computer control. Modules are scanned with the ^{137}Cs wire source at the time of assembly and installation. When the detector comes on line to take data, the movable source can be used to verify other calibration methods or to troubleshoot. We do not plan to perform source scans on a regular basis, so only two source drivers are needed at each detector site.

There are two source tubes per module, one at either end. The ^{137}Cs source is inserted into the source tube via a plastic funnel tube that is connected (temporarily) to the source tube and runs back to the ^{137}Cs storage unit. Source tubes traverse all of the scintillators in a module within 60 cm of the scintillator ends. The source tube at the end-cap is positioned near the right edge of a module. It runs parallel to the strip direction in the end-cap, but as the tube reaches the scintillator strips it is bent with a 25 cm radius across the strips. After a bend of 60° the source tube traverses the remaining scintillator strips in the module in a straight line. This permits all strips to be illuminated in approximately the same location and keeps the bend radius large enough so that the source will not stick in the tube.

5.4.6.4 Calibration module

The calibration module is essentially a "test beam calorimeter" built with final production components. This detector will be exposed to hadrons, electrons and muons using the planned Main Injector test beam at Fermilab in order to determine the absolute light response and energy resolution for hadronic and EM showers. The initial module will use summed outputs from detector planes to provide the necessary calibration at low cost. Most of the components, except for the steel and scintillator planes, will be spares from the near and far detectors. If oscillation signatures are observed, further understanding of details of the response and resolution can be obtained by upgrading the calibration module with the full transverse instrumentation as in the near and far detectors. The module will be transportable in order to cross-check the response of muons in the module at the different detector sites, if deemed necessary. The module will be equipped with a source and light calibration devices as in the main detectors.

The features of the proposed initial calibration module are:

1. The module has 40 layers of steel, each layer being 2.54 cm in thickness. The total thickness of iron is 102 cm or 5.9 interaction lengths. The number of layers has been set based on the containment of showers from 30 GeV pions.

2. The dimensions of the calibration module are 2.4 m (longitudinal) by 1.0 m (transverse) and 1.0 m (height) with a rectangular cross section. The transverse dimensions have been set to permit containment of events, even with the detector axis rotated by up to 60° with respect to the beam axis (assuming 20 cm offset to one side for the incident beam).

3. The detector weighs about 8 tons.

4. There are 41 layers of scintillator strips with 24 strips per detector plane. All features of the scintillator strip assemblies mimic the construction of the near and far detector in order to ensure the same response to showers. The orientation of the scintillator strips is rotated by 90° in successive planes.

5. Clear fiber ribbon cables transmit light to MUX boxes and photodetectors as in the near and far detectors.

6. The photodetectors are identical to those used in the near and far detectors. The scintillator strips are read out at one end. The output of 8 neighboring strips in each detector plane are multiplexed onto a single pixel of the photodetector. Hence, a total of 123 pixels are required for the full detector, corresponding to 8 phototubes.

5.4.6.5 Cosmic ray muons

The MINOS near and far detectors experience a flux of high energy muons produced high in the atmosphere in primary cosmic ray interactions. They offer the possibility of direct calibration in the low energy range of the MINOS scintillators using minimum ionizing particles. There are two principal questions: First, are the rates of these muons adequate for calibration, especially at the deep location at Soudan? Second, are there significant differences in the energy deposited in the scintillators at the two locations due to the different muon energy spectra and angular distributions?

The rates and angular distributions of the underground muons at Soudan are well-known[19]. Using these, we have calculated the flux and the muon path length distribution through a single 8 m long MINOS scintillator, 1 cm $\times$ 4 cm in cross-section and oriented at 45° to the horizontal. The muon flux is is 1000 ± 100 per month. The flux in the near detector will be 500 to 1000 times greater. The distribution of muon path lengths through the scintillator strips shows a well defined peak with median value 1.45 cm. Ten percent of the muons will have a path length greater than 3 cm.

The energy deposited in the scintillator strips is dependent on the muon energy spectra. This dependence can arise from the relativistic rise in dE/dx ionization loss as a function of primary energy, and also from differing bremsstrahlung, delta-ray, and pair production along the track of the muon. We have estimated the difference in average muon energy at the near and far detector halls. The median muon energy at Soudan 2 depth is 250 GeV and at Fermilab it is 40 GeV. We have estimated the average energy deposition rate in plastic scintillator due to ionization as a function of energy. Averaging over the muon energy distribution, we estimate that any difference between the two depths will be less than 1%. The probability of delta rays accompanying the muon is essentially energy independent and, indeed, is already accounted for in the the ionization prescription. Hence, the main concern for possible calibration differences are due to bremsstrahlung and pair production in the steel which sends extra particles into the scintillator strips.

The probabilities of bremsstrahlung, and pair production in the steel of the Soudan 2 detector have been calculated previously[19]. Energy losses via bremsstrahlung and pair production are strongly dependent on the muon energy. The former tends to produce large

bursts of energy relatively infrequently along the muon path. These electromagnetic showers have been studied in the Soudan 2 detector and will produce extremely large scintillator signals less than 3% of the time. They can be removed by a simple cut. However, the pair production process require more study.

We have made a Monte-Carlo calculation of photoelectron yields for muons at Soudan, based on the known angular and energy distribution of those muons and observed light output distributions for cosmic-ray muons in our prototype scintillator strips. Poisson statistics have been assumed for the observed photoelectron distribution. By calculating the mean on a truncated distribution, the Monte-Carlo calculation suggests that the light output of each scintillator strip can be calibrated to a precision of 2% in 1 month. In order to verify these estimates, we are undertaking a series of measurements at different depths underground, using scintillator strips located between 5 cm steel sheets.

Ultimately, if necessary, we can check the muon calibration at the different detector sites using the transportable calibration module. Finally, about 7% of the muons stop in the detectors. These will provide a source of muons of known energies (using range to determine energies) to provide another cross-check on the calibration.

5.4.6.6 Calibration plan

The goal of the calibration system is to permit the translation of the measured hadronic and EM shower response from a test beam to the near and far detectors and over the full time-period of data acquisition.

The calibration module will be used to obtain calibration data in a charged-particle test beam at Fermilab. Cosmic-ray muon data will be used to transport the calibration to the near and far detectors. The rate of cosmic ray muons is sufficiently low (especially at Soudan) that it is important to keep track of gain changes in the system over a shorter time scale. A 2% calibration for each far detector scintillator strip is possible with one month of muon data and an equivalent amount of data from the calibration module (at Soudan) will be required.

The near and far detector light injection systems provide the ability to track short-term gain changes and to measure the response curve to light of the full PMT/electronics system for each fiber independently. For each channel, a set of constants will be produced comprising a pedestal and one or more constants describing the shape of the light in/light out curve. The muon data provide a common fixed point in the light response curve for each fiber. The light-injection system also permits localization of any anomalies in light transmission through the fibers and connectors. The electronics is tested independently by direct injection of charge (see Chapter 6).

The above procedure provides a complete set of calibration information. However, we also have some cross-checks on this calibration. During installation the individual strips are tested with the ^{137}Cs source. This provides both an important debugging tool and a cross-check on the muon calibration of light output. At the near detector, through-going muons from neutrino events provide an independent data set for calibration. Finally, we could choose to operate the calibration module at the near detector site to obtain neutrino events. In this case, there will be a sufficient number of neutrino events in the calibration module to make a direct comparison of hadronic energy in those events to hadronic energy in the near detector target/calorimeter region.

5.4.7 Assembly and testing equipment (WBS 2.2.7)

Construction and testing of scintillator modules requires several specialized machines which are described in this Section.

5.4.7.1 Extrusion trimming machine

The extrusion trimming machine is used to cut the length of each scintillator strip to a tolerance of 1 mm. The trimming saw is a stock commercial cut-off saw equipped with a fine blade and an 12-m long custom cradle. This scintillator strip cradle has a graduated slide to enable a technician to quickly and precisely set the final length of the extrusion.

5.4.7.2 WLS fiber gluing machine

This Section describes the machine which glues WLS fibers and reflective groove covers to the scintillator strips using a commercial glue dispensing system. The operation of the machine in production mode is described in Section 5.4.8.2. Figure 5.27 shows the conceptual design for the gluing machine. The machine performs three completely automated operations on scintillator strips in one pass. It lays a bead of optical glue in the extrusion groove, places a WLS fiber in the glue bead, and lays the reflective extrusion groove cover over the fiber.

The machine requires operator assistance to set up a WLS fiber in an extrusion prior to gluing, and to cut and set the fiber after gluing. The machine transports strips lengthwise underneath three work heads. Scintillator strips, which have already been cut to length, are fed to the gluing machine from preloaded magazines. Magazines are used to provide a continuous supply of strips to the glue machine with minimal operator intervention.

Glued strips coming off the glue machine are placed in a curing rack which contains horizontally indexable shelves, each holding the 20 or 28 strips needed for a single module. After gluing the strips for one module, the operator adjusts the height of the curing rack to bring an empty shelf into alignment with the exit of the gluing machine.

The WLS fiber gluing machine contains five functional modules: a glue dispenser, a WLS fiber unwind stand, a reflective extrusion groove cover unwind stand, an extrusion feed mechanism, and a central programmable logic controller (PLC). In addition, the machine includes three auxiliary modules to perform quality control and inspection functions. The first auxiliary module checks for cracks in the WLS fiber cladding, the second measures the width of the scintillator strip at several points along its length, and the third tests the light output of the scintillator by shining a UV light into the groove and measuring the blue light emitted.

A commercially available glue dispensing system mixes the two parts of the glue in a specially designed disposable dispensing nozzle (replaced after each shift). The glue dispensing system meters the resin and hardener glue components (supplied from five gallon buckets) and is insensitive to variations in viscosity.

The WLS fiber and reflective groove cover unwind stands are equipped with commercially available tension controllers. The PLC matches the length of the glue bead dispensed to the length of the strip being processed. The central PLC controls both the glue dispenser and the unwind stand tension controllers.

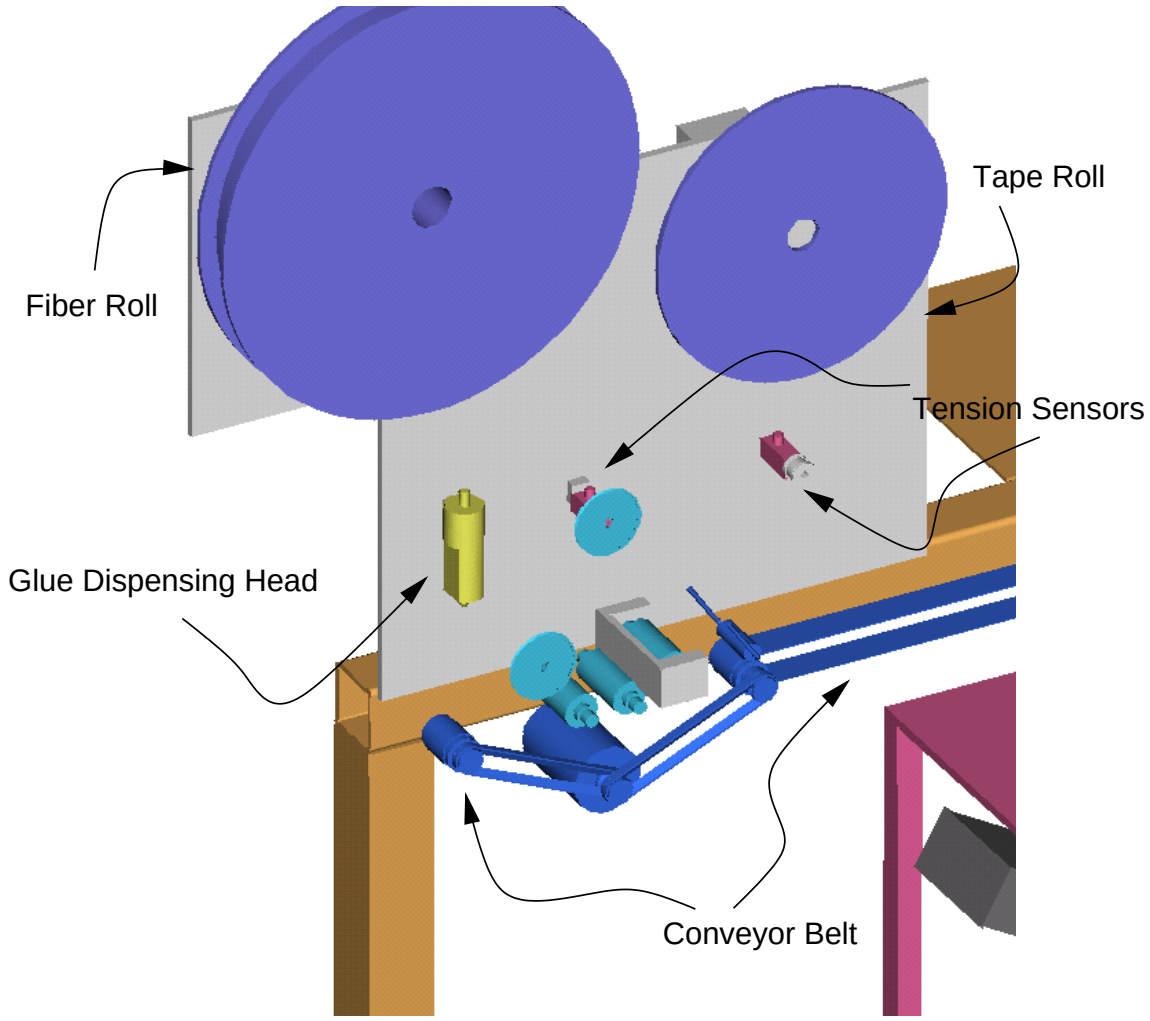

Figure 5.27: Conceptual design for WLS fiber gluing machine.

The curing rack holds the 96 strips required for one shift of assembly. The filled rack is moved to the assembly area when the glue has cured and the extrusions are ready for assembly into modules.

The WLS fiber gluing machine has a special accommodation for strips interrupted by the magnet coil bypass hole. The machine is equipped to glue one continuous WLS fiber across two extrusion sections, each approximately 4 m in length, for these modules. A dummy section of extrusion, matching the free fiber length required to clear the bypass hole, is temporarily placed between the two extrusion sections. The PLC shuts off the glue supply as the dummy section passes beneath the glue dispenser. The dummy section is removed after the glue cures, leaving the correct length of WLS fiber for routing around the bypass hole.

5.4.7.3 Scintillator/fiber gluing templates

The WLS fibers extend for some distance (enough to reach the optical connector) past each end of each scintillator extrusion, so the fiber extensions must be protected during gluing and handling (prior to installation in the module). Each scintillator strip is placed in an aluminum channel which is just large enough to hold the strip. In addition, extra pieces of actual scintillator strip are placed at each end of the strip being worked on. The end pieces are custom-length "tools" which hold the extra fiber (without glue) while the glue in the center strip cures. The entire assembly is run through the glue machine and the end pieces of scintillator are used to determine when to start and stop the glue flow. The fibers are clamped at the outside ends to hold them in place while the glue is curing. The very end of the fiber will be cut off after installation in the module and does not need to be protected.

5.4.7.4 Light case rolling machine

The module factory is equipped with a rolling machine to form the aluminum light case U channels. The machine allows the aluminum sheet for the light cases to be purchased in convenient roll form.

5.4.7.5 Module assembly tables

The module factory is equipped with two equivalent module assembly tables. The tables provide fixturing for technicians to manually assemble modules accurately and efficiently. The module assembly is done in two main stages. In the first stage, a bottom light case is placed on a support tray, scintillator strips placed in it on top of a glue layer, fibers are routed through the end manifolds and potted into connectors, and the top light case put into place on top of a second layer of glue. This assembly is sealed between two sheets of Mylar and evacuated with a mechanical vacuum pump in order to compress it uniformly while the glue sets. Following this, the modules are left overnight to allow the glue to cure completely. The following day, the aluminum case is crimped to produce a light-tight seal, the top manifold cover is installed, the manifold edges are glued, and the connectors are cut and polished.

5.4.7.6 Assembly table glue mixing machine

Substantial quantities of epoxy must be mixed to glue the scintillator strips to the top and bottom U channels of the light case. More epoxy is needed to glue the source calibration tubes to the light case. One automatic glue dispensing machine mixes the glue for both assembly tables. The machine has a mixing nozzle similar to that used on the WLS fiber gluing machine, but it is used only to supply precisely mixed batch lots of glue in disposable containers.

5.4.7.7 Optical connector polishing machine

A portable fly cutting machine is used to face the optical connectors utilized in the end manifolds of each module. Our application requires only minor modifications to the holding fixture of an existing Michigan State University machine to conform to MINOS connectors. The machine consists of a precision electrical motor with a fly cutter attached to its spindle. This assembly is affixed to a dove-tailed linear slide driven by a pneumatic piston. The fly cutter passes at right angles to a tool holder which grips the optical connector.

5.4.7.8 Curing racks

The module factory requires two styles of curing racks. The first holds groups of individual strips after they exit from the WLS fiber gluing machine, as described in Section 5.4.7.2. The second type of curing rack holds up to six trays that support assembled modules while the structural glue is curing.

Two sets of racks are required per shift. One set is filled with newly-glued components fabricated during the shift. The second set has strips or modules which were glued the previous day and are ready for the next steps in assembly.

5.4.7.9 Module mapper

The light yield due to variation in scintillator light output, attenuation length of WLS fibers and features of assembly could vary from batch to batch. Therefore it is important to quantify the response of each scintillator-fiber element within a module following the assembly. This map will be used for future understanding of the module performance and allow rejection of any modules which have poor response features. Furthermore, we will provide the capability to subject modules to a "quick-scan" at the detector sites prior to installation onto steel octagons in order to ensure that no damage has occurred during shipping and handling.

The module mapper is an automated device which consists of a large flat table with a collimated ^{137}Cs source that can be moved quickly to any location over the surface of the module. The response over a predetermined x-y grid will be measured for each module immediately following assembly. The source is located 5 mm above the module's skin. The distance between source and module skin will be controlled by a feedback mechanism.

Drawings of the module mapper are shown in Figures 5.28 and 5.29. The source is driven in two orthogonal directions: the long direction spans the full length of scintillator strips and the short direction spans the module width. The drive mechanism positions the source

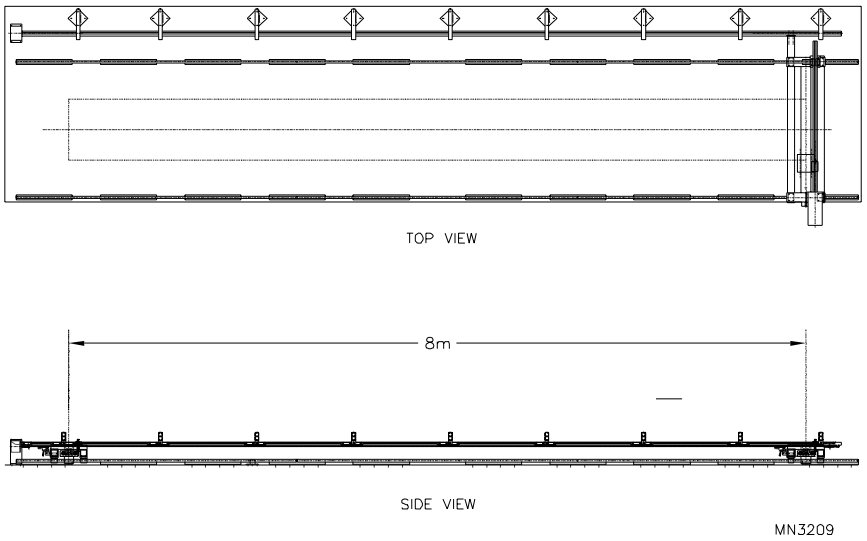

Figure 5.28: The module mapper. The top and side views of an 8 m long scintillator module are shown.

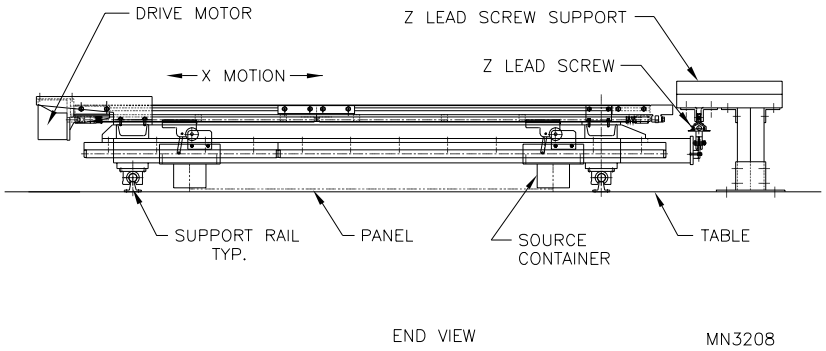

Figure 5.29: End view of mapper shows details of scanning device and the source container at two extreme positions.

with an accuracy of ± 1 mm in the short direction and ± 3 mm in the long direction. Drive speed is 30 cm/s in the long direction and 7.5 cm/s in the short direction.

Calibrated photodetectors are read out by the same processor that controls the source position. The response of each scintillator strip will be measured every 50 cm (or less, if necessary) along its length at the assembly factory. The capability will be provided to perform a quick-scan at the near and far detector sites using the module mapper. This will permit checks of module integrity following shipping as deemed necessary based on experience.

The response maps of each module will be entered in a database. As a cross-calibration, a radioactive source (see Section 5.4.6.3) will be inserted into the calibration tube at each module end and the response recorded in the database. This will permit an easy check that the module performance after installation in the detector is the same as when it was mapped.

5.4.8 Module factories (WBS 2.2.8)

The scintillator modules could be produced at a single production site running two shifts per day. However, we expect that the optimal production scenario will include two factory locations for module production. This permits faster production (and provides some schedule contingency) and efficient use of collaboration resources while keeping costs low. The layout and materials flow plan of the module factory are shown in Figure 5.30. The boxes correspond to the machines described in Section 5.4.7. The arrows indicate the flow of module components between machines. Each factory will have a seven person crew and will produce an average of four modules per shift. Module assembly tests have verified that this is a realistic rate for production. The following Sections describe factory operations in the order indicated in Figure 5.30.

5.4.8.1 Prepare scintillator strips

Scintillator strips are purchased in several lengths and are fine cut on the factory floor. Trimming is especially important for 45° angled modules, where the length of every extrusion in the module is different. During the trimming, the extrusion is visually inspected for any signs of external damage. The trimmed strips are loaded into magazines used to feed the WLS fiber gluing machine. Handling, inspection, trimming, and loading time is estimated at 2 minutes per extrusion.

5.4.8.2 Glue WLS fiber and reflective cover to extrusion

The WLS fiber gluing machine is operated by one technician. The gluing machine is fed by magazines of 20 to 28 strips to reduce the labor of loading each extrusion individually. Furthermore, the magazines help to preserve the order of strips cut to different lengths. Gluing templates with clamps are used to keep the fibers in place during glue curing and while feeding the strip through the machine. These also keep the scintillator piece from moving during the necessary handling. The machine glues the WLS fiber and attaches the reflective groove cover for the length of the extrusion. Once the fiber is glued and clamped, it is rough cut to an appropriate length beyond the end of the strip. The glue machine is also designed to test the quality of the fiber and scintillator strip as each pass through test points, prior to gluing. The average gluing time for each extrusion is estimated at two minutes per extrusion.

5.4.8.3 Prepare light case U channels

The light case U channels are formed from a roll of sheet aluminum using the light case rolling machine described in Section 5.4.7.4. The same machine is used for both the bottom and top U channels. The width of each light case can be adjusted to accommodate different widths of scintillator strips used in each module. The total time required for all operations associated with the rolling machine is estimated at 20 minutes per module. Rolling operations are performed by the same technician that operates the extrusion trimming station.

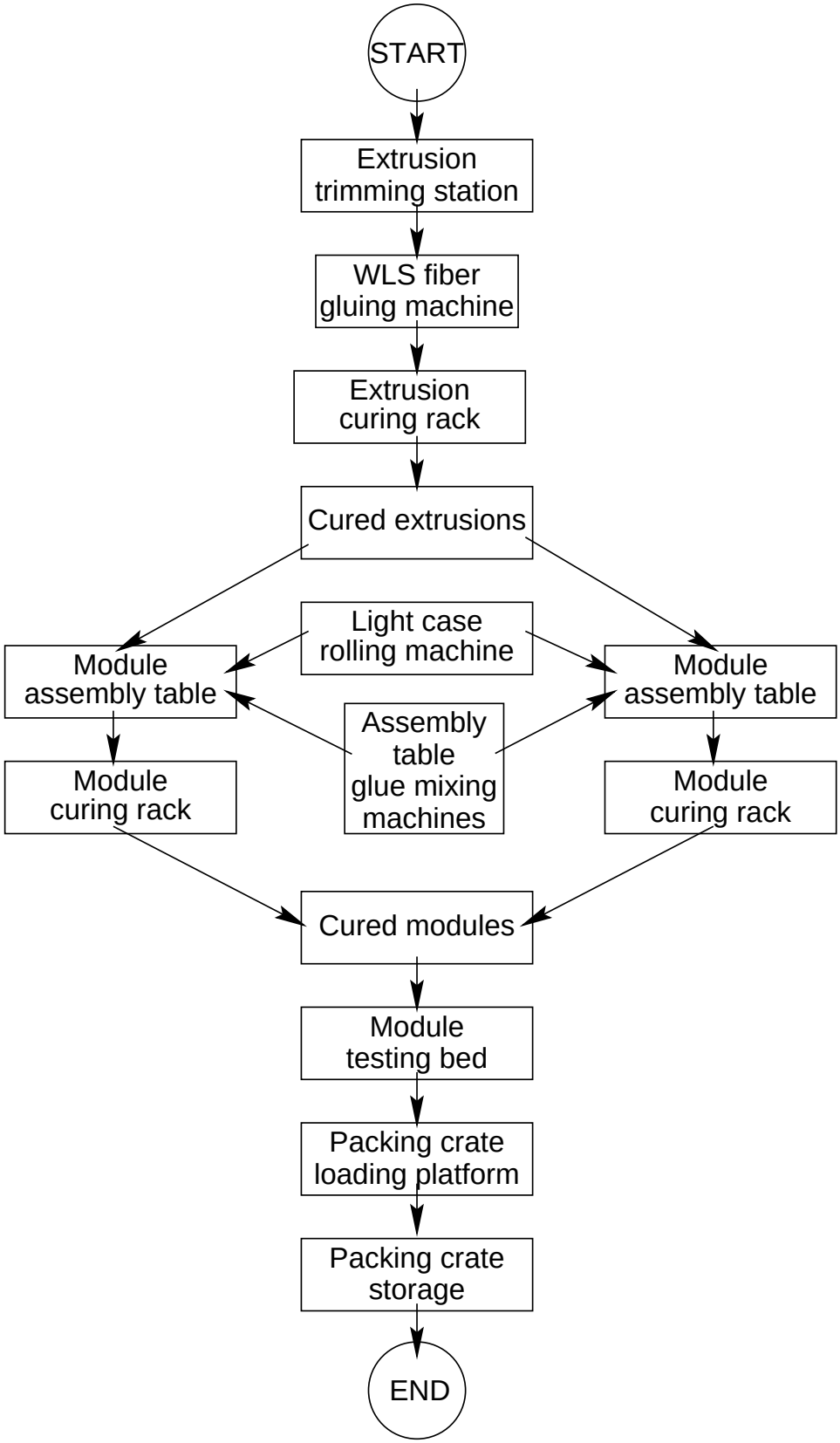

Figure 5.30: Floor plan of equipment layout and materials flow in module factory.

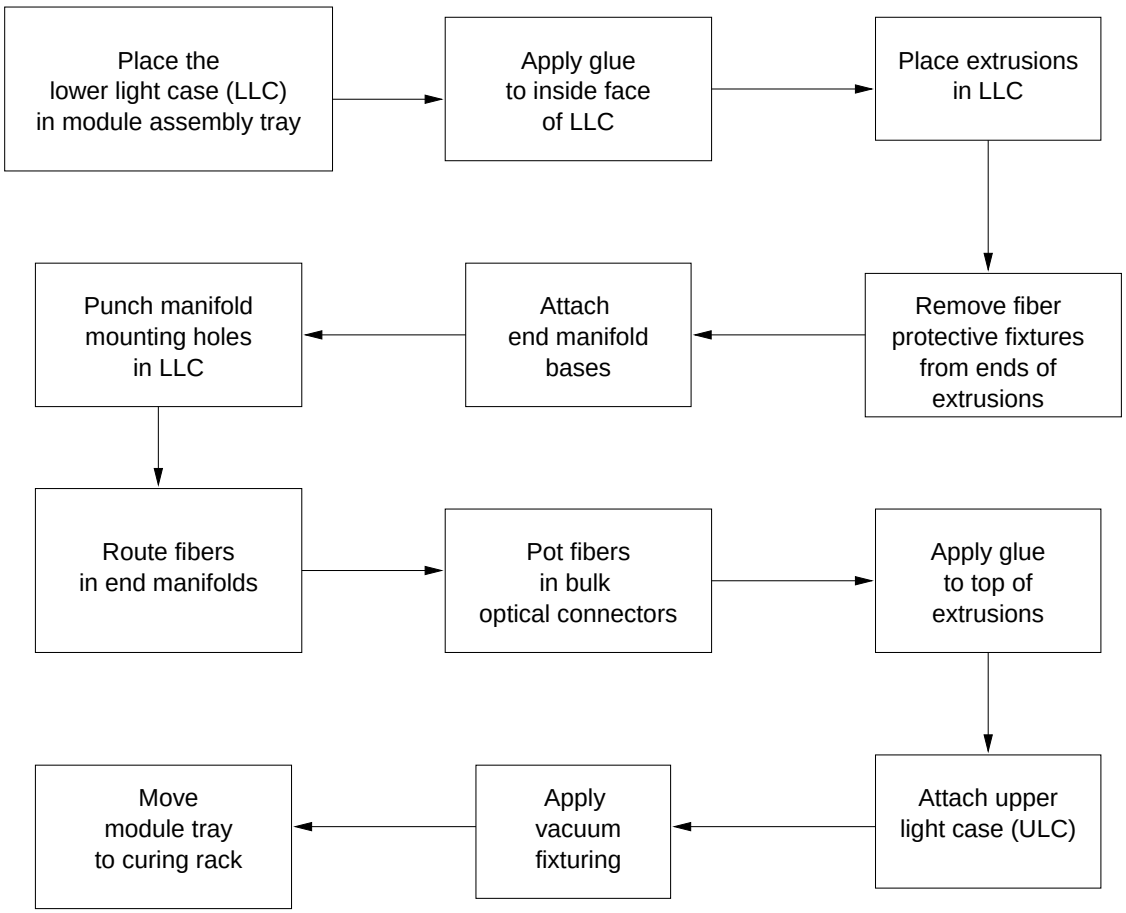

Figure 5.31: Flow chart of module assembly operations performed at the first stage of module assembly.

5.4.8.4 Assemble strips in light case and route fibers

The first step to assemble a complete module is to glue the strips into the aluminum light case and route the WLS fibers in the manifolds to the bulk optical connectors. The module is compressed using a vacuum table while the glue sets, and is then left overnight to allow the glue to cure completely. A flow chart of operations required for this stage is provided in Fig. 5.31. Most operations are self-explanatory. Two technicians are required for the operations in this step. Fibers are routed into the manifold and connector as each strip is layed into the bottom light case. This helps to keep fibers in order and protects them from damage. This step requires about one hour per module.

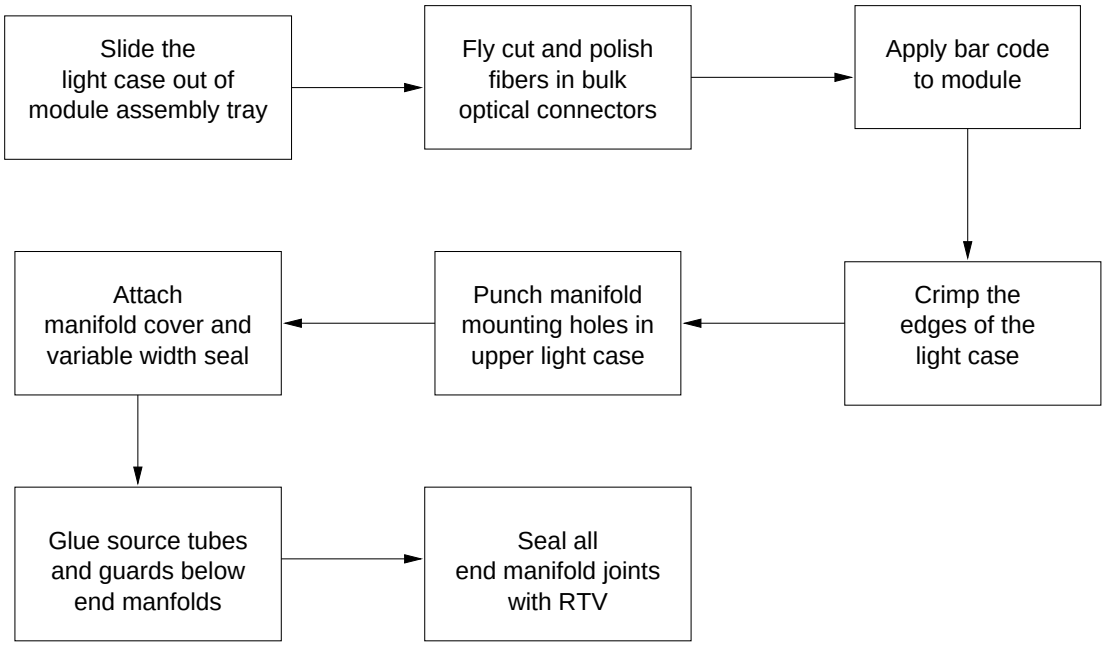

Figure 5.32: Flow chart of operations needed to complete module assembly.

5.4.8.5 Finish module assembly

Once the glue in modules has been allowed to cure overnight, the steps needed to finish the module assembly are done. A flow chart of operations required at this stage is provided in Fig. 5.32. Most operations are self-explanatory.

The portable optical connector polishing machine described in Section 5.4.7.7 is used to face all optical connector plugs in one module. The operations in this step are estimated to require a total of one hour per module

5.4.8.6 Source map module and light-leak check

Completed modules are moved to the source-mapping table for checks for light leaks and mapping with the radioactive source. Light leaks are detected by anomalously high count rates using slightly higher than normal ambient light levels. Any leaks are located using a bright local light and covered. When the module is light tight, the automated mapping machine is started and runs on its own. Each strip of the module is mapped at 50 cm intervals along the length. The computer controls the source location and collects data which are stored for future reference. Finally, the wire source is inserted at each end to establish the light yield response of the module for this source at the time of production.

5.4.8.7 Packing and shipping of modules

Shipping crates will be of a very rigid construction, fabricated from a combination of angle iron, 13 mm diameter steel rods, and plywood sheets. The deflection of the crates when picked up from the ends is approximately 6 mm. Modules are supported in the crate hori-

zontally. It is estimated that the modules can easily handle deflections of up to 25 cm over their length. The total weight of the largest crates and modules is approximately 6,000 lbs. There are two types of crates, one for each module width, with different lengths for near and far detector modules.

The crates will be insulated with 5 cm thick styrofoam which provides cushioning to the modules and insulates them from temperature extremes. It is expected that modules will be fabricated and shipped in temperature controlled conditions. However, during the transfer of crates from temperature controlled trucks to the underground entrance shaft, some crates are likely to be briefly subjected to temperatures as cold as -20° C. The insulated crates will prevent any possibility of damage during this transfer.

A total of 20 crates are needed during peak production and installation times to permit buffering of production and storage of modules at the near and far detector sites awaiting installation. The maximum weight that can be transported on a standard semi-trailer is 40,000 lbs, thus limiting each shipment to six full-size crates. Trucks delivering modules will pick up empty crates for delivery back to the module production factory.

5.4.8.8 MUX box assembly

The MUX boxes for MINOS will be assembled at two sites. These sites will require only a small amount of specialized equipment: a fly cutting machine, a computer controlled LED array and three PMTs for testing the boxes. Other equipment is assumed to exist at established laboratories. The MUX box front plate, chassis, chassis cover, back plate, and PMT cover box will be stamped and formed at a sheet metal shop. The cookie, cookie holder, and PMT holder will be fabricated by computer numerically controlled machines. The PMT jackets will be extruded.

The procedure for assembling the internal components of the MUX boxes includes the following steps:

1. The clear optical fibers are cut and trimmed to size, and then inserted and glued into the connectors.

2. With the aid of the computer controlled LED array, the fibers from the first group of 128 fibers are routed to the first cookie in the box and then glued into place.

3. The lacing pattern is tested using the computer controlled LED array.

4. The connectors and cookie are fly cut and polished.

5. The preceding three steps are repeated for the other two cookies in each box.

Prior to installation, PMTs are fit to PMT-holders and the assemblies are aligned with the cookie holders. The PMTs will be installed at the detector sites to reduce any chance of damage. Once PMTs are installed, the whole readout chain from the optical inputs at the front plate to the signal outputs at the electronics is tested, channel by channel using the programmable LED array.

5.4.9 Management (WBS 2.2.9)

Two of the scintillator system managers are engineers and require salary support for the fraction of time which they spend on management activities. This effort is estimated to be one month per year.

Several managers require travel support for regular interactions with the Fermilab management, other MINOS managers and interaction with the collaboration and vendors. Specific travel allocations have been made for the scintillator Level 2 manager and for the module, assembly equipment and factory managers. In addition, several "generic" trips per year have been allocated for other members of the scintillator management staff.

5.5 Future optimization and engineering

5.5.1 Purpose and goals

The scintillator system described in this Chapter is a complete design which meets the physics requirements specified for MINOS, using demonstrated technology and known costs. However, the engineering of the system, including essential large-scale prototyping, must be completed prior to proceeding with production. The baseline design is now at a stage where fine tuning of components is under way. This fine tuning is aimed at obtaining the best possible light output and at reducing production costs. Some examples of fine-tuning design changes we have already adopted are:

- Scintillator fluor concentration: Our studies have shown that a 0.03% concentration of POPOP gives 10 to 15% more light output than the old baseline of 0.015% POPOP (which had initially been determined from cast samples). The cost impact of this change is minimal and is an excellent value for the gain in light output. Large scale assemblies with strips made with 0.03% POPOP will be built within the next two months.

- "In-line" fluor infusion: We have recently developed a technique for mixing fluors into polystyrene as the scintillator strips are extruded rather than in a separate step. It is estimated that the one-step, or "in-line" process saves about $1M in the production cost of scintillator. We note that this single cost savings is more than all the R&D funds we have spent on the development of the scintillator system to date.

- Fiber diameter: Based on a series of measurements of light collection in our scintillator with different fiber diameters, we have decided that 1.2 mm fiber is optimal for MINOS. This maximizes light output and use of the effective area of the phototube pixels in the Hamamatsu M16 PMT. It is possible that some small additional tuning of the fiber diameter will be optimal for light transmission at connectors.

We note that, during the last year, our "fine tuning" of the baseline design has resulted in about a factor of two increase in light output. We anticipate that there are additional improvements on the order of a few tens of percent to the light output which will be realized in the next few months of additional fine tuning. Examples of such work now under way are

further studies of scintillator production techniques, optimizing the design of the bulk optical connectors, fine tuning of the thickness of the scintillator, optimizing the manifold design and production techniques, and fine tuning of module design and construction techniques. An activity of increasing importance as we head towards production is involvement of industrial suppliers in the production of our components. We are working with potential industrial suppliers to ensure that we will have a cost-effective and reliable supply of components for module assembly.

The schedule for scintillator optimization and engineering is set by the requirement of having modules ready for prompt installation as soon as occupancy in the near and far detector halls permits. We have used the January 2001 date for occupancy of the far detector hall for purposes of planning the schedule for scintillator engineering and startup of production. Our schedule includes the following milestone dates:

- **Nov. 1998:** Lehman Review of baseline design.
- **Oct. 1998 - June 1999:** Fine tuning of detector components. Small modifications to the baseline design such as exact fiber diameter (1.0 to 1.2 mm with or without steps at connectors), thickness of scintillator (1.0 to 1.2 cm), design of connectors and manifolds, etc. will be studied and considered for potential cost savings or improvement in light output.
- **June 1999:** Review light output and modifications to design. Decide all design issues. Start final engineering of design.
- **Nov. 1999:** Final review and approval of engineering design.
- **Dec. 1999:** Place first commercial orders for assembly prototype (at Fermilab).
- **Jan. 2000:** Start factory setup. Produce modules for assembly tests.
- **June 2000:** Place orders for components for first supermodule.
- **Oct. 2000:** Ramp-up production of modules for first supermodule.
- **Dec. 2000:** Two planes of modules at Soudan, ready for installation.
- **Mar. 2001:** Scintillator module production at full rate.

The following activities will be pursued during the engineering and optimization phase:

1. Extruded scintillator production: We will continue to work with both industrial plastics extruders and scintillator manufacturers to improve light output and/or decrease the cost for extruded scintillator. Due to the industrial nature of this process, any iteration in the production technique takes a minimum of 3 months. The optimization includes possible small changes in the geometry of scintillator strips to improve light output and/or collection.
2. Wavelength-shifting fibers: We have found some batch variation in WLS fibers delivered over the last two years, and are working with manufacturers to define testing standards for long fibers in order to improve their quality control.

3. Scintillator module construction: Additional work on engineering and prototyping will be undertaken to ensure understanding of construction issues and to arrive at an optimal design for cost. Full size prototypes are being constructed and tested for light output and mechanical properties. Full-scale planes of scintillator will be assembled on prototype steel octagons and mounted as in the final detector to ensure that all integration issues have been understood.

4. Clear fiber ribbon cables: We must establish production of clear fiber cables which meet the needs for MINOS. We will arrange orders from Mitsubishi and Kuraray and Chinese vendors. An attractive possibility is to have the complete clear-fiber assemblies produced by our IHEP Beijing collaborators.

5. Connectors: We are investigating a custom-built optical connector for MINOS which is based on designs built for other experiments.

6. Photodetectors: The baseline photodetector is the Hamamatsu M16. This device meets all of the technical requirements of the proposed physics measurements, for the cost stated in our baseline documentation[1]. Our future work with this tube will further develop our understanding of tube-to-tube variations in response, in parallel with testing of improved versions of the tube which Hamamatsu is continuously developing. We have performed considerable R&D work to compare the possibility of using an HPD (hybrid photodiode) rather than the M16 PMT. The use of an HPD offers some potential advantages compared to the PMT due to various technical differences, including better intrinsic stability and uniformity of HPD photon response compared to PMTs. We have not identified any sufficiently large advantage of the HPD for MINOS which would justify changing our baseline design. Some work continues on study of the HPD as a possible design contingency to the baseline.

7. Calibration: A complete calibration system has been described for MINOS, based on experience and specific designs used in previous calorimeters. However, there are several aspects of deployment in MINOS where further reductions in cost are possible with additional optimization work.

8. Aging tests: Most detectors built with solid scintillator display a mild drop in light output as a function of time due to yellowing and other aging effects. The light output of the MINOS baseline design is high enough that the sensitivity of physics measurements will not be degraded by such effects. Although the MINOS scintillator design incorporates a number of features which have not been used in earlier experiments, all of the components of our scintillator modules have been used in previous detectors with no significant problems due to aging. However, we must ensure that new features of the MINOS application do not introduce an unacceptable rate of decrease in light output versus time. We have already begun a program of aging tests to demonstrate the long-term stability of all of our components and assemblies.

9. Full-plane prototypes: In order to understand system integration issues we will assemble a series of full-size prototype planes of scintillator, mounted on steel octagons,

and will study these with calibration systems and cosmic rays as part of the 4-plane prototype studies in the New Muon Lab at Fermilab (see Sections 4.4.5 and 7.5.1).

10. Test beams studies: In order to ensure that the full system works as expected, test beam measurements of hadron calorimetric response will be made (see Section 5.5.3).

5.5.2 Aging tests

Long term effects of various stresses on the scintillator strip assemblies are being studied. The aging tests are planned to continue for the next several years to quantify the effects of aging. We have placed fibers, scintillator strips, glue samples and full scintillator/fiber/glue assemblies in several aging conditions including:

- High temperature (50°C).
- Cycled temperature (-30°C to +50°C every 4 hours).
- High temperature + high humidity (50°C and 90% relative humidity).
- Mechanical stress (assembled strips bend around a 2.0 m radius).

The main effects have been observed in high temperature and for fibers high humidity as well. Aging in the glue has a negligible effect (due to the thin layers which will be used in MINOS). Aging in both the scintillator and fibers contributes to a slow drop in light output at high temperature. In 8 months of aging at 50°C we have observed a drop in light output of about 30 to 35% in complete assemblies. The expected acceleration factor is around 10 (or more) so that this corresponds to about 80 months of aging at normal temperature. We have concluded that we can expect less than a factor of two drop in light output over a period of ten years.

5.5.3 Test beam studies

Should signatures of neutrino oscillations be observed in MINOS, it will be of interest to reduce all systematic errors as much as possible in order to get the best precision in oscillation parameters. In this case, it will be of interest to undertake an expanded effort on test beam measurements beyond that described in Section 5.4.6.4. We anticipate that with such an effort, the systematic uncertainty in the absolute energy scale in the near and far detectors could be reduced to less than 2%. In addition, more detailed information on the topology of showering events in the detector could be obtained. The plan is that the calibration module will be built from modules with connectors identical to those used in the near and far detectors. By simply purchasing additional photodetectors and electronics, it will be possible to instrument the calibration module with the full transverse granularity as in the near and far detectors. This would also help to check for any systematic effects which might arise due to differences in summing of signals between the initial calibration module and the near and far detectors.

In addition to the extra instrumentation, the calibration module could also be magnetized in order to provide a direct measurement of the change in response in this condition. Previous

measurements have shown that the response of hadronic showers can change when the iron is magnetized[20, 21]. To first order, the change can be corrected without a direct measurement.

Finally, it will be possible to move the calibration module to the near and far detector sites. In both locations, data from cosmic ray muons could be collected and compared to ensure a complete understanding of the energy deposition at the two sites. In addition, neutrino events could be measured at the near site and compared to those observed in the near detector target/calorimeter region.

Chapter 5 References

[1] Detailed costs and schedules corresponding to the design described in this Chapter are given by the Fermilab NuMI Project Staff in "NuMI Project Cost and Schedule Plan," October 1998, Fermilab report NuMI-362.

[2] M. Adams *et al.*, Nucl. Instr. Meth. **A366**, 263-277 (1995).

[3] M. Adams *et al.*, Nucl. Instr. Meth. **A378**, 131-142 (1996).

[4] Kuraray Co., Methacrylic Resin Division, 8F, Maruzen Building, 3-10, 2-Chome, Hihonbashi, Chuo-ku, Tokyo, 103-0027, Japan. Kuraray America Inc., 200 Park Avenue, New York, NY 10166.

[5] Quick Plastics, 3530 Wayland Dr., Jackson, MI 49202.

[6] Polycast and Royalite are divisions of Uniroyal. Royalite Thermoplastics 2001 W. Washington St., P.O. Box 1836, South Bend, IN 46634. Polycast Technology Corporation, 70 Carlisle Place, Stamford, CT 06902.

[7] Dow Chemical Company, 2040 Dow Center, Midland, MI 48674.

[8] Chroma Corporation, 3900 Dayton St., McHenry, IL 60050.

[9] Bicron Corp., 12345 Kinsman Road, Newbury, Ohio 44065.

[10] G. Apollinari, P. de Barbaro and M. Mishina, "CDF End Plug Calorimeter Upgrade Project", Fermilab-Conf-94/030-E, CDF note 2432.

[11] M. Chung and S. Margulies, "Aging studies on stressed and unstressed scintillating, wave-shifting and clear fibers," Proceedings of SPIE 2551, 2-9 (1995).

[12] Epon is a trade name for Epoxy resin manufactured by Shell.

[13] Manho Chung, University of Illinois, Chicago, DO Collaboration, private communication.

[14] Hamamatsu Photonics K.K., 325-6, Sunayama-cho, Hamamatsu City, 430, Japan, U.S. Main Office: 360 Foothill Road, P.O. BOX 6910, Bridgewater, NJ 08807-06910.

[15] The HERA-B experiment at DESY is designed to study B meson decays produced by 800 GeV protons striking an internal thin wire target. Two types of photomultipliers are employed by HERA-B ring imaging Cerenkov counter: Hamamatsu R5900U-00-M16 and M4. There are 1500 M16 tubes and 750 M4 tubes used.

[16] CDF collaboration, The CDF II Detector, Technical Design Report, November 1996.

[17] J. Bahr *et al.*, Nucl. Instr. Meth. **A330**, 103 (1993).
G. Apollinari *et al.*, Nucl. Instr. Meth. **A324**, 475 (1993).
Yu. Bonushkin *et al.*, Nucl. Instr. Meth. **A381**, 349 (1996).
M. Lindgren *et al.*, Nucl. Instr. Meth. **A387**, 53 (1997).

[18] DDK electronics, 3001 Oakmead Village Dr., Santa Clara, CA 95051.

[19] S. Kasahara, Ph.D. thesis, U. Minn (1997).
K. Ruddick, "Underground particle fluxes in the Soudan mine," NuMI-L-210.
R.K. Menon and R. Murthy, Prog. Elem. Part. and C.R. Phys., **9**, 162, (1967).

[20] S. Kunori, "B-Field effects on scintillator and calorimetry," VII International Conference on Calorimetry in High Energy Physics, Nov. 1997, Tucson, AZ.

[21] V.V. Abramov, Nucl. Instr. Meth. **A374**, 34 (1996).